Geochimica et Cosmochimica Acta, Vol. 68, No. 24, pp. 5081–5101, 2004

0016-7037/04 $30.00 + .00

doi:10.1016/j.gca.2004.08.029

Sulfur speciation and network structural changes in sodium silicate glasses: Constraints from NMR and Raman spectroscopy

TOMOYUKI TSUJIMURA, XIANYU XUE,*† MASAMI KANZAKI, and MICHAEL J. WALTER‡
Institute for Study of the Earth's Interior, Okayama University, Misasa, Tottori, 682-0193, Japan

(*Received January* 20, 2004; *accepted in revised form August* 30, 2004)

Abstract—Information about the state of sulfur in silicate melts and glasses is important in both earth sciences and materials sciences. Because of its variety of valence states from S^{2-} (sulfide) to S^{6+} (sulfate), the speciation of sulfur dissolved in silicate melts and glasses is expected to be highly dependent on the oxygen fugacity. To place new constraint on this issue, we have synthesized sulfur-bearing sodium silicate glasses (quenched melts) from starting materials containing sulfur of different valence states (Na_2SO_4, Na_2SO_3, $Na_2S_2O_3$ and native S) using an internally heated gas pressure vessel, and have applied electron-induced SKα X-ray fluorescence, micro-Raman and NMR spectroscopic techniques to probe their structure. The wavelength shift of SKα X-rays revealed that the differences in the valence state of sulfur in the starting compounds are largely retained in the synthesized sulfur-bearing glasses, with a small reduction for more oxidized samples. The ^{29}Si MAS NMR spectra of all the glasses contain no peaks attributable to the $SiO_{4-n}S_n$ (with $n > 0$) linkages. The Raman spectra are consistent with the coexistence of sodium sulfate (Na_2SO_4) species and one or more types of more reduced sulfur species containing S-S linkages in all the sulfur-bearing silicate glasses, with the former dominant in glasses produced from Na_2SO_4-doped starting materials, and the latter more abundant in more reduced glasses. The ^{29}Si MAS NMR and Raman spectra also revealed changes in the silicate network structure of the sulfur-bearing glasses, which can be interpreted in terms of changes in the chemical composition and sulfur speciation. *Copyright © 2004 Elsevier Ltd*

1. INTRODUCTION

Sulfur constitutes an important volatile component in natural magmas. Knowledge of the solubility and speciation of sulfur in silicate melts is important for the understanding of a variety of geological processes such as the formation of sulfide ore deposits, volcanic sulfur emissions and elemental cycling. The behavior of sulfur in silicate melts and glasses is also of interest for radioactive waste storage and industrial glass refining. Sulfur exhibits a variety of valences, from −2 to + 6, in natural minerals and synthetic materials. A large number of sulfur species have been recognized, including groups containing sulfur of a single valence state, such as sulfate (SO_4^{2-}), sulfite (SO_3^{2-}), dithionate ($[O_3S\text{-}SO_3]^{2-}$), dithionite ($[O_2S\text{-}SO_2]^{2-}$), elemental sulfur (S_8) and sulfide (S^{2-}), and those of two or more different valence states, such as thiosulfate ($[S(O_3\ S)]^{2-}$), metabisulfite ($[O_2S\text{-}SO_3]^{2-}$), polythionates ($[O_3S\text{-}(S_n)\text{-}SO_3]^{2-}$) and polysulfides ($[S\text{-}(S_n)\text{-}S]^{2-}$) (cf. Wells, 1986). Thus, the solubility and speciation of sulfur in silicate melts and glasses are expected to be complicated and depend on the oxidation state.

There have been extensive experimental and theoretical studies on sulfur solubility in silicate melts of simple and natural compositions (Fincham and Richardson, 1954; Abraham et al., 1960; Shimazaki and Clark, 1973; Nagashima and Katsura, 1973; Haughton et al., 1974; Katsura and Nagashima, 1974; Shima and Naldrett, 1975; Danckwerth et al., 1979; Buchanan and Nolan, 1979; Mysen and Popp, 1980; Wendlandt, 1982; Carroll and Rutherford, 1985, 1987; Luhr, 1990; Poulson and Ohmoto, 1990; O'Neill and Mavrogenes, 2002). The results have often been interpreted by the dissolution of sulfur in the melts as sulfide and sulfate species, with the former dominant at relatively low oxygen fugacities (f_{O2}), and the latter becoming important at relatively high f_{O2}. These species have generally been assumed to be coordinated with network-modifying cations, such as Na. The following equation has been invoked to describe their equilibrium:

$$S^{2-}(\text{melt}) + 2O_2(\text{gas}) = SO_4^{2-}(\text{melt}) \quad (1)$$

The proportions of S^{2-} and SO_4^{2-} species as a function of f_{O2} have been estimated for a number of silicate glasses of natural and synthetic compositions from the SKα X-ray wavelength shift (e.g., Carroll and Rutherford, 1988; Wallace and Carmichael, 1992, 1994) and wet chemical analysis (e.g., Nagashima and Katsura, 1973; Katsura and Nagashima, 1974). X-ray absorption near-edge spectroscopic (XANES) studies of natural and synthetic glasses support the presence of these species (e.g., Paris et al., 2001). A more recent X-ray microspectroscopic study of natural olivine-hosted glass inclusions identified, in addition, sulfur in the form of sulfite (S^{4+}) (Métrich et al., 2002, 2003).

Several spectroscopic studies on the speciation of sulfur in silicate, borosilicate and borate glasses have also been published in the materials science literature. Ahmed et al. (1980, 1997) have studied several binary alkali borate glasses doped with sulfur or Na_2S with UV-visible absorption and Raman spectroscopic techniques, and suggested that the following sulfur species are present depending on the glass composition: S_3^-, S_2^- and S_x^{2-} (x = 2∼6), and that the colors of these

* Author to whom correspondence should be addressed (tujimura@misasa.okayama-u.ac.jp).
† Research center, Asahi Glass Co., Ltd. 1-1 Svehiro, Tsurumi, Yokohama, 230-0045, Japan.
‡ *Present address:* Department of Earth Sciences, University of Bristol, Bristol, BS8 1RJ, United Kingdom.

glasses are related to the state of sulfur. Tatsumisago et al. (1996) studied glasses in the Li_2S-SiS_2-Li_4SiO_4 system with ^{29}Si magic-angle spinning nuclear magnetic resonance (MAS NMR) spectroscopy and observed peaks near −55 and −25 ppm, in addition to those expected for SiS_4 and SiO_4 groups, and attributed these additional peaks to SiO_nS_{4-n} (n = 1 to 3) groups. Asahi et al. (1998) studied glasses synthesized from Na_2S-SiO_2 with both ^{29}Si MAS NMR and X-ray photoelectron spectroscopy (XPS), and identified two similar peaks in the ^{29}Si-NMR spectra, in addition to those expected for the SiO_4 groups. Our recent ab initio molecular orbital calculations (Xue and Kanzaki, 2004a) suggested that these peaks are due to SiO_3S (near −55 ppm) and SiO_2S_2 (near −25 ppm) groups. Asahi et al. (1998) also inferred that some of the sulfur could be present as sodium sulfide clusters in the more sodium-rich glasses. Konijnendijk and Buster (1977) have studied several sodium, potassium, and calcium silicate glasses doped with sulfates, and McKeown et al. (2001) studied borosilicate glasses doped with sulfates, both with Raman spectroscopy. Both studies identified a strong Raman peak near 990 cm^{-1}, and attributed it to the symmetric S-O stretching mode of SO_4^{2-}. Very recently, McKeown et al. (2004) studied the sulfur speciation in borosilicate and other glasses with XANES, and concluded that while most glasses contain sulfate as the major species, some synthesized under reducing conditions yield complicated features that may indicate the presence of sulfate, sulfite, and more reduced species. However, unambiguous identification and quantification of the latter species have been found difficult from XANES alone. These studies thus suggest that sulfur could be present in a variety of species depending on the glass composition and oxidation state. It is also clear that our understanding of sulfur speciation in silicate melts and glasses is far from complete and that a systematic study of silicate glasses synthesized under a range of oxidation states, using a combination of different spectroscopic techniques, is desirable, to gain a better understanding of this complicated problem.

In this study, we have investigated the sulfur speciation in sodium silicate glasses (quenched melts) synthesized from starting materials containing sulfur of different valence states (Na_2SO_4, Na_2SO_3, $Na_2S_2O_3$ and native S), using electron-induced SKα X-ray fluorescence, micro-Raman and ^{29}Si, ^{1}H and ^{23}Na MAS NMR spectroscopy. The Na_2O-SiO_2 system was chosen because of its good glass-forming ability and because the Raman and NMR features are well understood from extensive past studies. Instead of directly controlling the oxygen fugacity of the synthesis condition, starting materials containing sulfur of different valences were used to gain insight into the effect of oxidation state on sulfur speciation. The valence state of sulfur in the synthesized sulfur-bearing glasses can be evaluated using the wavelength of SKα X-rays determined using an electron microprobe (Carroll and Rutherford, 1988). Raman spectroscopy is useful for identifying the various species of sulfur (cf. Nakamoto, 1986) and may also place constraints on the Si Q^n (SiO_4 tetrahedra with n nearest SiO_4 neighbors) speciation distribution (e.g., Furukawa et al., 1981). ^{29}Si MAS NMR is unique in identifying and quantifying Si of different types or numbers (coordination) of first neighbors, and can also give information about their second neighbor connectivities, such as the Si Q^n speciation (cf. Kirkpatrick, 1988).

2. EXPERIMENTAL PROCEDURES

2.1. Sample Preparation

The $Na_2O \cdot xSiO_2$ (x = 1.5, 2, 2.3 and 3) starting glasses have been prepared from dried Na_2CO_3 and SiO_2 powders by mixing under acetone, then decarbonizing at 750°C for 12 h, followed by melting at 1200°C for 2 h in a platinum crucible. ~0.2 wt% Gd_2O_3 was added to some of the samples, prepared for ^{29}Si MAS NMR measurement, to shorten the ^{29}Si spin-lattice relaxation time (T_1). All the glasses, with or without Gd_2O_3, were colorless, and were confirmed to be clear and homogeneous from optical microscopic and micro-Raman spectroscopic examinations. These glasses have been freshly prepared for each series of experiments, to avoid complications arising from water absorption on stored samples.

The sulfur-containing sodium silicate glasses have been synthesized from mixtures of $Na_2O \cdot xSiO_2$ glass plus one of the following: sodium sulfate (Na_2SO_4), sodium sulfite (Na_2SO_3), sodium thiosulfate ($Na_2S_2O_3$), native sulfur (S), graphite(C), and native sulfur plus graphite. Graphite was used as a reducing agent for some of the experiments. The appropriate amounts of starting materials were mixed and welded shut into a metal capsule. Samples were held at 1000°C (for Au capsules) or 1300°C (for Pt capsules) and 960 to 1970 bar for a desired duration, and then quenched to glasses under pressure in an internally heated argon-pressured vessel (IHPV) with a rapid quenching device. The experimental conditions are summarized in Table 1.

It has been reported that sulfur tends to react with most noble metal capsules, such as Pt, Ag and Pd, although no measurable sulfur loss was observed using Au capsules (see Keppler, 1999). We have performed some test experiments to evaluate this problem. For experiments using Na_2SO_4-doped starting materials, no reactions were observed between the sample and either of the Pt or Au capsules. For experiments employing native sulfur-doped starting materials, no signs of reactions were found between the sample and Au capsule from back-scattered electron image of the recovered samples, but severe reactions were observed when a Pt or Au-Pd capsule was employed. Thus, we have adopted Au capsules for all subsequent experiments using native sulfur-doped starting materials.

To establish the appropriate run duration needed to achieve equilibrium, we have performed test experiments for two starting compositions of $Na_2O \cdot 2SiO_2$ + 8.7 wt% Na_2SO_4 and $Na_2O \cdot 2SiO_2$ + 8.8 wt% S, with run durations from 4 h to 24 h. No differences were observed in the chemical compositions, analyzed using an electron microprobe, or in the Raman spectra for the glasses synthesized with different run durations, confirming that equilibrium was reached at run durations above 4 h. A run duration of 8 h has been adopted for all the reported results. No spatial heterogeneities were detected within the glass phase of all the samples from Raman and electron microprobe analyses.

To check whether 0.2 wt% Gd_2O_3 has a significant effect on the glass structure, we have conducted parallel experiments for some of the $Na_2O \cdot 1.5SiO_2$ + Na_2SO_4 samples, with and without 0.2 wt% Gd_2O_3 added, under otherwise identical conditions. The Raman spectra of the two series of samples were identical, suggesting that the added Gd_2O_3 has no significant effects on the glass structure.

The run products synthesized from starting materials containing Na_2SO_4, $Na_2S_2O_3$, and Na_2SO_3 were all clear and homogenous glasses, as confirmed by both optical microscopic and micro-Raman spectroscopic examinations. Those synthesized from native sulfur-doped starting materials all contained homogeneous glasses covered by a yellowish liquid that gave off a strong odor of hydrogen sulfide when the capsule was first opened. The liquid solidified, within about 1 to 2 d after the sample was taken out of the capsule, to a faint reddish yellow ($Na_2O \cdot xSiO_2$-S; x = 1.5, 2) or yellow ($Na_2O \cdot 3SiO_2$-S) material. Inclusions of ~1 μm in diameter were also observed inside some of the glasses under an optical microscope. Thus, the compositions of these samples are most likely within the silicate melt-fluid immiscibility region at the pressure and temperature conditions of syntheses. In the run products obtained from graphite-containing starting materials, fine graphite particles were also identified inside the glass under an optical microscope.

All the sulfur-containing glasses were colored. Glasses synthesized from $Na_2O \cdot 1.5SiO_2$ + Na_2SO_4 all exhibited faint red colors, and those from $Na_2O \cdot 2SiO_2$ + Na_2SO_4 showed faint reddish yellow colors, both

Table 1. Experimental conditions and starting materials for all sulfur-bearing glasses.

Sample	Experimental condition		Starting glass[a]	Added materials (wt%)
	Temperature (°C)	Pressure (bar)		
a501	1000	1970	NS1.5a-gd	Graphite (1.2%) + native S (5.0%)
e002	1000	990	NS1.5b-gd	Graphite (1.2%)
e003	1000	990	NS1.5b-gd	Graphite (1.2%) + native S (1.0%)
d007	1000	990	NS2	Native S (0.5%)
d009	1000	990	NS2	Native S (1.9%)
d010	1000	990	NS2	Native S (2.9%)
d011	1000	990	NS2	Native S (5.5%)
d057	1000	1970	NS2a-gd	Native S (8.8%)
b301	1000	1950	NS2.3-gd	Graphite (1.2%) + native S (5.0%)
e024	1000	1970	NS1.5c-gd	Na_2SO_4 (2.5%)
e025	1000	1970	NS1.5c-gd	Na_2SO_4 (2.9%)
e026	1000	1970	NS1.5c-gd	Na_2SO_4 (6.0%)
d035	1300	1970	NS2b-gd	Na_2SO_4 (1.6%)
d036	1300	1970	NS2b-gd	Na_2SO_4 (4.6%)
d037	1300	1970	NS2b-gd	Na_2SO_4 (7.5%)
d038	1300	1970	NS2b-gd	Na_2SO_4 (8.1%)
e031	1000	1970	NS1.5d	Na_2SO_3 (3.8%)
e032	1000	1970	NS1.5d	$Na_2S_2O_3$ (4.5%)
tr030	1000	1970	NS3-gd	Native S (5.0%)
tr031	1000	1970	NS3-gd	Native S (2.9%)
e051	1000	1970	NS1.5e	Native S (6.7%)
e052	1000	1970	NS1.5e	Native S (3.0%)
e053	1000	1970	NS1.5e	Na_2SO_4 (6.0%)
e054	1000	1970	NS1.5e	Na_2SO_4 (3.0%)

[a] NS1.5 = $Na_2O \cdot 1.5SiO_2$; NS2 = $Na_2O \cdot 2.0SiO_2$; NS2.3 = $Na_2O \cdot 2.3SiO_2$; NS3 = $Na_2O \cdot 3.0SiO_2$; gd = 0.2 wt% Gd_2O_3 doped; a, b, c, d, and e denote separate batches of starting glasses.

of which deepen with increasing Na_2SO_4 content. Glasses synthesized from $Na_2O \cdot 1.5SiO_2 + Na_2S_2O_3$ or Na_2SO_3 both exhibited red color, with the former deeper than the latter. Glasses synthesized from $Na_2O \cdot xSiO_2$ (x = 1.5, 2, 2.3) + S were red, and those from $Na_2O \cdot 3SiO_2$ + S were faint reddish yellow. Glasses synthesized from $Na_2O \cdot xSiO_2$ (x = 1.5, 2.3) + S + C were reddish black.

2.2. Chemical Analyses and SKα Chemical Shift Measurements

We have measured the chemical compositions and wavelength of the SKα fluorescence X-ray line with a JEOL JXA-8800 electron microprobe. Polished sections of the samples were prepared using oil (DP-Lubricant from Struers) to avoid sample hydration. Electron microprobe analysis of sodium silicate glasses is known to be difficult because of easy electron beam damage and Na_2O-loss of the glasses. We have thus tested various measurement conditions using a soda-lime container glass sample of NBS 621 standard. Na_2O-loss was found to arise when a high-beam current (20 nA) is used, but could be avoided by using a low-beam current (0.77 nA). With the latter beam current, the analyzed chemical compositions of the glasses vary little with the accelerated voltage between 12.5 and 15.0 kV or beam diameter between 10 and 50 μm. An accelerating voltage of 12.5 kV, a beam current of 0.77 nA, a counting time of 120 s and beam diameter of 20 μm have been adopted for all the reported results. Wider beam diameters are not desirable, especially for glasses containing sulfur-bearing inclusions. Five points have been measured for each sample and the average values are reported. The composition for the soda-lime container glass sample of NBS 621 standard, analyzed with this method, is within analytical uncertainty of that certified.

We have measured the wavelength of the SKα fluorescence X-ray line for all the glasses using the same electron microprobe to estimate the oxidation state of sulfur, following Carroll and Rutherford (1988). These analyses were performed with step-scan using a step size of 0.00005 in sin θ unit and a counting time of 9 s at each step. For the glass samples, the electron beam must be moved to a new spot after each step during the scan to avoid beam damage. For reference, spectra for crystalline barite ($BaSO_4$), sodium sulfite (Na_2SO_3), orthorhombic sulfur (S), sphalerite (ZnS), pyrrhotite ($Fe_{1-x}S$) and galena (PbS) were also acquired, and the peak positions are reported relative to that of galena. The SKα peak positions for these reference compounds show a systematic shift with increasing average oxidation state of sulfur, from 0 Å for sulfides, to -1.08×10^{-3} Å for orthorhombic S, to -2.32×10^{-3} Å for sulfite, and to -3.06×10^{-3} Å for sulfate (see Table 2). Our measured shift between barite and galena is similar to those reported previously between anhydrite and pyrrhotite ($3.08 \pm 0.08 \times 10^{-3}$ Å Carroll and Rutherford, 1988), between barite and pyrrhotite ($3.1 \pm 0.1 \times 10^{-3}$ Å Métrich and Clocchiatti, 1996), between barite and galena ($3.1 \pm 0.1 \times 10^{-3}$ Å Gurenko and Schmincke, 2000) and between $SrSO_4$ and galena ($3.07 \pm 0.02 \times 10^{-3}$ Å Yasuda et al., 2001).

The sulfur contents for some of the glasses have also been determined by ion chromatography. Only the results for homogeneous glass samples synthesized from starting materials of $Na_2O \cdot xSiO_2$ (x = 1.5, 2) plus Na_2SO_4 are reported, because those for glasses produced from native sulfur-doped starting materials are complicated by the coexistence of a sulfur-bearing yellowish material.

2.3. ^{29}Si, ^{1}H and ^{23}Na MAS NMR Spectroscopy

We have conducted ^{29}Si, ^{1}H and ^{23}Na MAS NMR measurements using a Varian Unity-Inova 400 MHz spectrometer at a Larmor resonance frequency of 79.5, 105.9 and 400.4 MHz, respectively. Chemical shifts were calibrated against an external standard of tetramethyl silane (TMS) for ^{29}Si and ^{1}H, and 1*M* aqueous NaCl for ^{23}Na. All the ^{29}Si MAS NMR spectra were acquired on samples doped with 0.2 wt% Gd_2O_3, and the ^{1}H and ^{23}Na MAS NMR spectra were obtained on samples both doped and not doped with Gd_2O_3. A 5-mm Jakobsen-type probe was used for all the NMR measurements. This probe gives a large ^{1}H signal, and a small broad ^{29}Si signal, both from outside the sample coil. Thus, most of the ^{29}Si and ^{1}H MAS NMR spectra have been acquired with the DEPTH sequence that consists of three back-to-back pulses ($\pi/2$-π-π) with a phase cycle of 16 (Cory and Ritchey, 1988). With this pulse sequence, the probe background signal becomes

Table 2. Summary of analyzed compositions and SKα wavelength shifts for glasses.

Sample	Added materials (wt%)	Added components (wt%)		Electron microprobe result (wt%)			S (I.C.)[a] (wt%)	$\Delta\lambda$(SKα) (Å $\times 10^3$)[b]
		Na_2O	S	SiO_2	Na_2O	S		
NS1.5a-gd				61.0 (0.5)	39.7 (0.4)			
a501	Graphite (1.2) + native S (5.0)		5.0	61.5 (0.2)	38.1 (0.8)	1.4 (0.1)		−0.33 (0.28)
NS1.5b-gd				59.4 (0.5)	40.0 (0.4)			
e002	Graphite (1.2)			59.2 (1.3)	39.0 (0.6)			
e003	Graphite (1.2) + native S (1.0)		1.0	59.8 (0.9)	39.8 (0.6)	0.5 (0.1)		−0.35 (0.24)
NS2				64.4 (0.4)	35.7 (0.4)			
d007	Native S (0.5)		0.5	65.2 (0.7)	33.2 (1.1)	0.4 (0.2)		−0.90 (0.22)
d009	Native S (1.9)		1.9	64.6 (0.2)	32.9 (2.1)	0.9 (0.1)		−0.86 (0.13)
d010	Native S (2.9)		2.9	65.3 (0.5)	32.3 (0.6)	0.9 (0.1)		−0.93 (0.21)
d011	Native S (5.5)		5.5	67.1 (1.6)	28.4 (1.2)	1.1 (0.1)		−1.34 (0.14)
NS2a-gd				66.0 (0.4)	34.2 (0.4)			
d057	Native S (8.8)		8.8	70.1 (0.5)	29.3 (0.9)	1.1 (0.1)		−0.98 (0.16)
NS2.3-gd				69.0 (0.9)	30.3 (0.6)			
b301	Graphite (1.2) + native S (5.0)		5.0	72.6 (0.8)	29.1 (0.0)	0.9 (0.0)		−0.65 (0.31)
NS1.5c-gd				60.1 (0.6)	38.5 (1.1)			
e024	Na_2SO_4 (2.5)	1.1	0.6	59.2 (1.6)	38.3 (0.7)	0.5 (0.1)	0.5	−2.31 (0.25)
e025	Na_2SO_4 (2.9)	1.3	0.6	58.9 (0.9)	39.4 (1.4)	0.5 (0.0)	0.6	−2.22 (0.23)
e026	Na_2SO_4 (6.0)	2.6	1.3	56.4 (1.0)	39.1 (0.9)	1.2 (0.1)	1.1	−2.44 (0.11)
NS2b-gd				67.1 (0.3)	31.6 (1.2)			
d035	Na_2SO_4 (1.6)	0.7	0.4	65.5 (1.0)	31.7 (1.4)	0.2 (0.1)	0.2	−2.01 (0.29)
d036	Na_2SO_4 (4.6)	2.0	1.0	64.5 (0.9)	31.6 (1.6)	1.1 (0.2)	0.9	−2.65 (0.14)
d037	Na_2SO_4 (7.5)	3.3	1.7	59.9 (2.0)	33.9 (1.7)	1.6 (0.0)	1.5	−2.74 (0.21)
d038	Na_2SO_4 (8.1)	3.5	1.8	60.4 (1.4)	32.9 (0.7)	1.8 (0.0)	1.6	−2.93 (0.16)
NS1.5d				60.7 (1.0)	38.9 (0.3)			
e031	Na_2SO_3 (3.8)	1.9	1.0	59.2 (0.7)	39.2 (0.6)	0.9 (0.1)		−1.81 (0.09)
e032	$Na_2S_2O_3$ (4.5)	1.8	1.8	58.7 (1.0)	39.8 (0.6)	1.6 (0.1)		−1.31 (0.15)
NS3-gd				74.2 (0.7)	24.8 (0.4)			
tr030	Native S (5.0)		5.0	75.6 (0.7)	23.9 (0.6)	0.7 (0.1)		−1.43 (0.52)
tr031	Native S (2.9)		2.9	74.6 (1.0)	23.0 (0.6)	0.6 (0.1)		−1.18 (0.45)
NS1.5e				61.0 (1.4)	40.8 (0.7)			
e051	Native S (6.7)		6.7	63.4 (0.6)	35.2 (0.2)	1.8 (0.1)		−0.73 (0.23)
e052	Native S (3.0)		3.0	61.2 (0.0)	39.3 (0.4)	1.3 (0.2)		−0.65 (0.27)
e053	Na_2SO_4 (6.0)	2.6	1.4	55.7 (1.6)	43.0 (0.8)	1.2 (0.2)		−2.33 (0.24)
e054	Na_2SO_4 (3.0)	1.3	0.7	59.6 (1.4)	40.2 (1.1)	0.6 (0.2)		−2.27 (0.19)

[a] Results from ion chromatography;
[b] SKα wavelength shift measured relative to galena. The measured values for crystalline compounds are: 0.00 (0.05) for galena (PbS); 0.00 (0.10) for pyrrhotite ($Fe_{1-x}S$); −0.01 (0.10) for sphalerite (ZnS); −0.17 (0.11) for pyrite (FeS_2), −1.08 (0.02) for orthorhombic S; −2.32 (0.14) for sodium sulfite (Na_2SO_3); −3.06 (0.08) for barite ($BaSO_4$).

negligible for ^{29}Si, and minor for ^{1}H; the latter was acquired each time on the empty rotor and subtracted from the reported spectra of the sample (see Xue and Kanzaki, 2004b). For all the NMR spectra, the linear prediction algorithm in the Varian VNMR software has been used to reconstruct signal loss during a short period of 'dead time'.

The ^{29}Si T_1 values for all the glasses doped with 0.2 wt% Gd_2O_3, measured with the saturation-recovery pulse sequence, are ~10 to 30 s. No significant differences were observed in the ^{29}Si T_1 values of different peaks in a given spectrum. The ^{29}Si MAS NMR spectra reported were mostly acquired with the DEPTH pulse sequence with a $\pi/2$ pulse of ~4.6 μs, a spectral width of 100 kHz, a delay time of 30 ~ 60 s, and a spinning rate of 8 kHz. Longer delay times were also used for some of the samples to check for changes in peak shape, and no differences were found within signal-to-noise ratios.

The ^{1}H MAS NMR spectra have been obtained to check for the content and speciation of water in the starting glasses and sulfur-bearing samples. These spectra were acquired using the DEPTH sequence with a $\pi/2$ pulse of 4 μs, a spectral width of 1 MHz, a spinning rate of 10 kHz, and a range of delay times between 5 to 120 s. Total water content in the sample was quantified from the integrated intensity of fully relaxed spectra, calibrated against those of hydrous silicate glasses of known water content (see Xue and Kanzaki, 2004b).

The ^{23}Na MAS NMR spectra have been acquired using a single pulse sequence, with a solid $\pi/6$ pulse of 0.7 μs, a spectral width of 1 MHz, a delay time of 1 s, and a spinning rate of 10 kHz.

2.4. Raman Spectroscopy

We have acquired unpolarized Raman spectra on glass fragments of ~2~3 mm in diameter using an argon-ion laser with a wavelength of 514.5 nm and a power of 20~40 mW. The incident light was directed normal to the sample surface in backscattering geometry, and focused to a spot size of 2 ~ 5 μm by a 10× objective lens. Light scattered from the sample was focused onto the entrance slit of an imaging spectrograph (f = 500 mm) equipped with a 1200 g/mm grating and a liquid nitrogen-cooled CCD detector. The Raman shift was calibrated using a Neon lamp in most experiments, although coesite, anhydrite and calcium carbonate were used in some early experiments. The Raman spectra have been acquired in the range of 82 to 1458 cm^{-1}; intensities below ~200 cm^{-1} are likely unreliable, due to the effect of notch filters used to reject the intense Raleigh scattering. Each spectrum was typically recorded for a duration of ~900 ~ 1000 s for glass samples, and ~60 s for the sulfur-containing material adhered on the surface of glasses synthesized from native sulfur-containing starting materials.

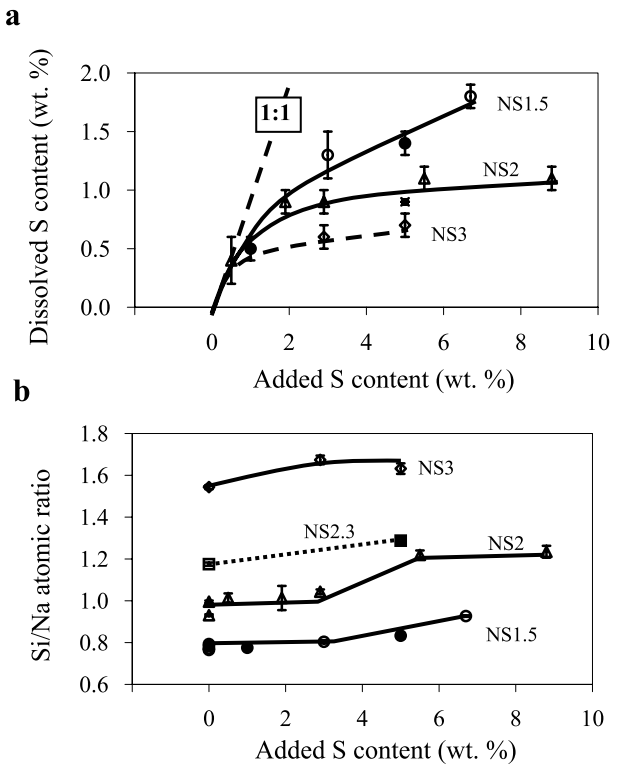

Fig. 1. The dissolved S content (wt%) (a), and Si/Na atomic ratio (b) from electron microprobe analysis, as a function of the added sulfur content (wt%) for glasses synthesized from $Na_2O \cdot xSiO_2$ + S mixtures. Solid and dotted lines are guides to the eyes. Circle: x = 1.5; triangle: x = 2.0; square: x = 2.3: diamond: x = 3.0; solid symbol: graphite-containing; open symbol: graphite-free.

3. RESULTS AND DISCUSSIONS

3.1. Chemical Composition and Sulfur Oxidation State

The analytical results for the chemical compositions of the glasses determined using electron microprobe and ion-chromatography are summarized in Table 2. The chemical compositions for all the starting $Na_2O \cdot xSiO_2$ (x = 1.5, 2, 2.3 and 3) glasses from electron microprobe analysis are within about ± 2 wt% (oxide component) of the respective nominal compositions. For glasses synthesized from sodium sulfate, sulfite or thiosulfate-doped starting materials, the analyzed sulfur contents from electron microprobe and ion chromatographic analyses agree well with those added to the starting materials, consistent with the homogeneous nature of these samples. As described above, samples produced from native sulfur-doped starting materials contain a yellowish material on the surface and interior of the glass. For the electron microprobe analysis of glasses in these samples, particular attention was paid to select regions free from the yellowish material. Qualitative electron microprobe analyses were also carried out on the yellowish material in two of the samples synthesized from starting materials of $Na_2O \cdot 2SiO_2$ plus native sulfur (d011, d057), which revealed only peaks of S and Na, but not Si. In Figure 1a, the dissolved sulfur contents in glasses synthesized from native sulfur-containing starting materials, from electron microprobe analysis, are plotted as a function of those added to the starting materials. The analyzed sulfur contents for these glasses are in general lower than those added, even at relatively low sulfur contents, consistent with the coexistence of the yellowish sulfur-bearing material. For a given starting silicate composition, the dissolved sulfur contents show an initial increase with added sulfur content, and then gradually level off above ~3 wt% added sulfur. The dissolved sulfur contents also vary with the silicate composition of the starting material, and are higher for less silica-rich compositions. The analyzed Si/Na atomic ratio for glasses synthesized from native sulfur-containing starting materials is plotted against the added sulfur content in Figure 1b. The Si/Na ratios of glasses for a given starting silicate composition are relatively constant when the added sulfur contents are low, but show a small increase above ~3 to 5 wt% added sulfur, consistent with the partitioning of some of the sodium into the coexisting phase. The variation in the dissolved sulfur content for these glasses cannot be explained by two-liquid immiscibility in a binary silicate-sulfur system, and may reflect more complicated immiscibility behavior in a multi-component (perhaps Na_2O-SiO_2-S) system.

The results of the SKα wavelength shift for sulfur-bearing glasses are summarized in Table 2. The SKα peak position for these glasses shifts systematically with the valence state of sulfur in the starting material, from $-0.6 \sim -1.4 \times 10^{-3}$ Å for native sulfur, to -1.3×10^{-3} Å for $Na_2S_2O_3$ and -1.8×10^{-3} Å for Na_2SO_3, and then to $-2.0 \sim -2.9 \times 10^{-3}$ Å for Na_2SO_4. Thus, the differences in sulfur valence state in the starting materials are largely retained in the synthesized sulfur-bearing glasses. For glasses synthesized from Na_2SO_4 and Na_2SO_3-doped starting materials, the SKα chemical shifts are in general less negative than those of the starting materials, indicating more reduced valence state of sulfur. Such a reduction is likely caused by penetration of H_2 through the metal capsule from the pressure medium, due to the presence of impurities in the argon and/or gases trapped on the inner wall of the IHPV apparatus. Glasses synthesized from $Na_2O \cdot 1.5SiO_2$ + Na_2SO_4 show somewhat less negative SKα chemical shift values ($-2.2 \sim -2.4 \times 10^{-3}$ Å), indicating greater reduction, than those from $Na_2O \cdot 2SiO_2$ + Na_2SO_4 ($-2.0 \sim -2.9 \times 10^{-3}$ Å). For glasses synthesized from native sulfur-doped starting materials, the SKα chemical shifts are less negative than native sulfur (-1.08×10^{-3} Å) for the $Na_2O \cdot 1.5SiO_2$ series (near -0.7×10^{-3} Å), but more negative for the $Na_2O \cdot 3SiO_2$ series ($-1.2 \sim -1.4 \times 10^{-3}$ Å), and either way for the $Na_2O \cdot 2SiO_2$ series ($-0.9 \sim -1.3 \times 10^{-3}$ Å). Interpretations of these variations are complicated by the unknown valence state of sulfur in the coexisting fluid phase. Glasses synthesized from starting materials containing both native sulfur and graphite yield SKα chemical shifts ($-0.3 \sim -0.7 \times 10^{-3}$ Å) clearly less negative than those without graphite described above, confirming the reducing effect of the added graphite.

3.2. ^{29}Si, ^{1}H and ^{23}Na MAS NMR Results

3.2.1. ^{29}Si MAS NMR Results

The ^{29}Si MAS NMR spectra for the starting $Na_2O \cdot xSiO_2$ (x = 1.5, 2, 2.3, 3) glasses (Fig. 2 to 6) are all similar to those reported for glasses of similar compositions, and each contain two to three components, near −77 ppm attributable

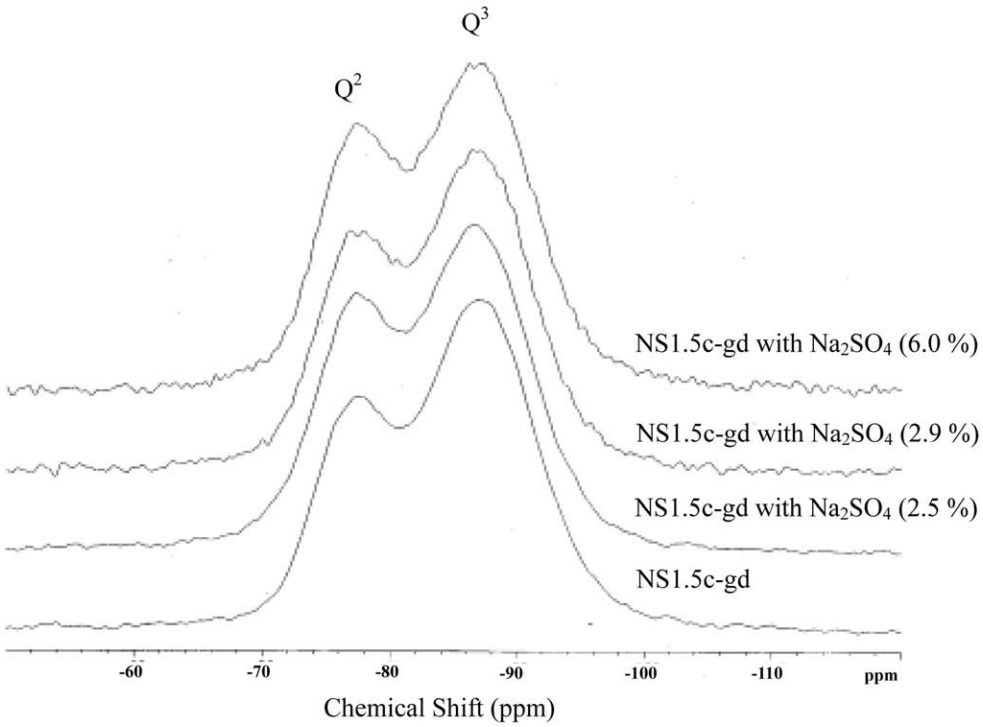

Fig. 2. ^{29}Si MAS NMR spectra for the starting $Na_2O \cdot 1.5SiO_2$ glass and sulfur-bearing glasses synthesized from $Na_2O \cdot 1.5SiO_2 + Na_2SO_4$, all with 0.2 wt% Gd_2O_3. The sulfur-free glass was quenched from melts at 1200°C and ambient pressure, and the sulfur-bearing glasses were quenched from melts at 1000°C and 1970 bar using the same batch of starting material. The labeled value in brackets is the added Na_2SO_4 content (wt%) in the starting material.

to the Q^2 species, near −88 ppm attributable to Q^3 species, and near −100 ppm attributable to the Q^4 species (e.g., Dupree et al., 1984; Maekawa et al., 1991).

The ^{29}Si MAS NMR spectra for the homogeneous glass samples synthesized from $Na_2O \cdot 1.5SiO_2 + Na_2SO_4$ and $Na_2O \cdot 2SiO_2 + Na_2SO_4$ are shown in Figure 2 and 3. For both series of samples, spectral changes are subtle, with a slight decrease in the relative intensity of the Q^4 to Q^3 peak ($Na_2O \cdot 2SiO_2$-Na_2SO_4 series), or Q^3 to Q^2 peak ($Na_2O \cdot 1.5SiO_2$-Na_2SO_4 series) with increasing added Na_2SO_4 content, suggesting that the glass structures are slightly less polymerized for the sulfur-bearing glasses.

The ^{29}Si MAS NMR spectra for samples produced from $Na_2O \cdot 1.5SiO_2$ + S (with or without graphite), $Na_2O \cdot 2SiO_2$ + S and $Na_2O \cdot 3SiO_2$ + S starting materials are shown in Figure 4 to 6, and those for samples produced from $Na_2O \cdot 2.3SiO_2$ + S are not shown. Although these samples all contain a yellowish material, in addition to the glass, the ^{29}Si MAS NMR spectra reflect only signals from the glass because the yellowish material contains no Si, as revealed by qualitative electron microprobe analysis and Raman spectra (see the next section). The relative intensity of the Q^3 to Q^2 peak for the $Na_2O \cdot 1.5SiO_2$-C-S series of samples, and that of the Q^4 to Q^3 peak for the other series, increase significantly with increasing dissolved sulfur content, suggesting that the glass structure becomes more polymerized. No differences were observed between the spectrum of the starting $Na_2O \cdot 1.5SiO_2$ glass and that of a glass synthesized from graphite-doped starting material (see Fig. 4).

We have quantified these results by fitting the ^{29}Si MAS NMR spectra with two to three gaussian peaks, representing the Q^2, Q^3 and Q^4 species. For the glasses of the $Na_2O \cdot xSiO_2$ (x = 1.5, 2.3, 3) compositions, the spectra can be deconvoluted without constraints because of the reasonable separation of different peaks. For the spectra of sulfur-free and some of the sulfur-bearing $Na_2O \cdot 2SiO_2$ glasses, constraint was necessary because of the weak intensity of the peak for Q^4 that partially overlaps with the main peak of Q^3. From the deconvolution results for the spectra of the other compositions, we have found that the full-widths-at-half-maximum-height (FWHM) of peaks for a give Q^n species do not show appreciable variation with composition (see Table 3), as was also reported in previous studies (e.g., Maekawa et al., 1991). The FWHM of the Q^4 peak was thus fixed to a value of 12.9 ppm during deconvolution of these spectra. The spectral range for both the central band and the spinning sidebands has been included for the deconvolution. The deconvolution results and the estimated bulk NBO/T are summarized in Table 4. The estimated bulk NBO/T values for the sulfur-free glasses are within ± 0.6 of those expected from the respective compositions. The estimated bulk NBO/T values for glasses produced from Na_2SO_4-doped starting materials show a small increase with increasing dissolved sulfur content (see Fig. 7a), and those of the glasses synthesized from native sulfur-doped starting materials shows a large decrease (see Fig. 7b).

As mentioned in the Introduction, peaks near −55 ppm and −25 ppm have been previously observed in glasses synthesized from Li_2S-SiS_2-Li_4SiO_4 and Na_2S-SiO_2 at ambient pressure (Tatsumisago et al., 1996; Asahi et al., 1998), and our recent ab

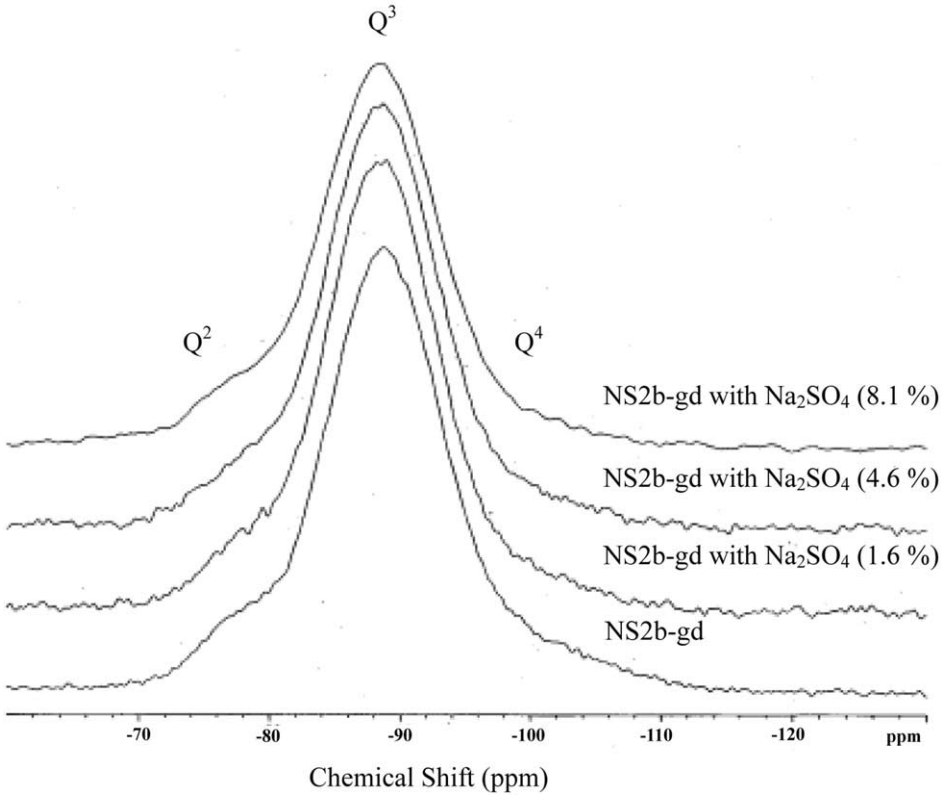

Fig. 3. ^{29}Si MAS NMR spectra for the starting $Na_2O \cdot 2SiO_2$ glass and sulfur-bearing glasses synthesized from $Na_2O \cdot 2SiO_2 + Na_2SO_4$, all with 0.2 wt% Gd_2O_3. The sulfur-free glass was quenched from melt at 1200°C and ambient pressure, and the sulfur-bearing glasses were quenched from melts at 1300°C and 1970 bar using the same batch of starting material. The labeled value in brackets is the added Na_2SO_4 content (wt%) in the starting material.

initio calculations (Xue and Kanzaki, 2004a) suggested that these peaks are due to SiO_3S (near −55 ppm) and SiO_2S_2 (near −25 ppm) groups. However, no discernible peaks near these positions are observed in all the spectra described above (see Fig. 5, 6 for examples). To evaluate the characteristics of these peaks, we have prepared another sample from $3Na_2S \cdot 7SiO_2$ at 1000°C and 1970 bar using the IHPV apparatus. Like samples synthesized from $Na_2O \cdot xSiO_2$ + S starting materials, this sample is composed of a yellowish sulfur-bearing glass covered by a heterogeneous sulfur-bearing, but silicon-free material condensed from the coexisting fluid. A small peak near −60 ppm with a FWHM of ~15 ppm is clearly recognizable, although no peak is visible near −25 ppm, in the ^{29}Si MAS NMR spectrum of this sample. Using the parameters for this peak as constraints, the proportions of Si as the SiO_3S group are estimated to be below ~0.7%, contributing to <0.3 wt% of sulfur, in all our samples synthesized from starting materials of $Na_2O \cdot xSiO_2$ plus Na_2SO_4 or S.

3.2.2. ^{1}H and ^{23}Na MAS NMR Results

We have acquired ^{1}H MAS NMR spectra only at the late stage of the study. In particular, a series of experiments (NS1.5e series in Table 1) have been carefully designed to evaluate the possible problems of hydration during sample preparation and high-pressure experiment. The more silica-poor $Na_2O \cdot 1.5SiO_2$ composition was chosen for this purpose,

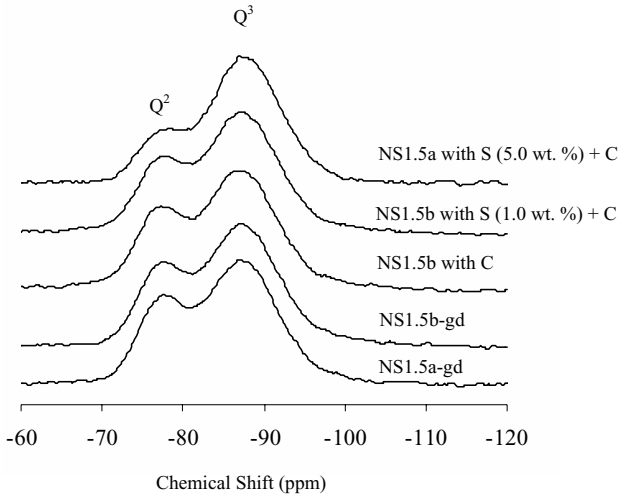

Fig. 4. ^{29}Si MAS NMR spectra for the starting $Na_2O \cdot 1.5SiO_2$ glass and samples synthesized from $Na_2O \cdot 1.5SiO_2$ + S with or without graphite and with 0.2 wt% Gd_2O_3. Two batches of starting glasses (NS1.5a-gd and b-gd), both quenched from melts at 1200°C and ambient pressure, were used. The sulfur-bearing samples were quenched from melt + fluid at 1000°C and 990 or 1970 bar and consist of a homogeneous glass phase and a yellowish Si-free material condensed from the fluid. The labeled value in brackets is the added sulfur content (wt%) in the starting material.

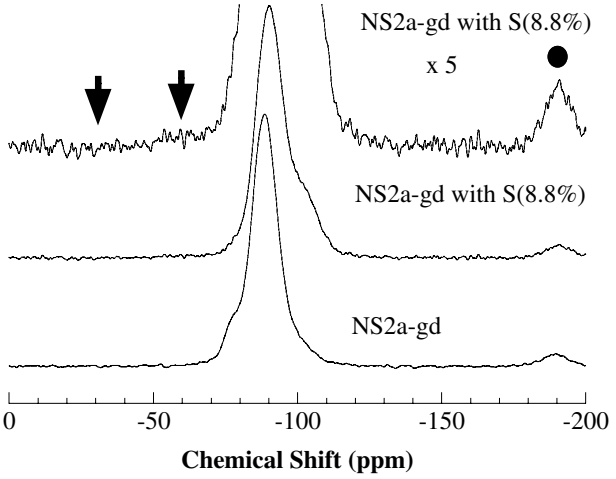

Fig. 5. ^{29}Si MAS NMR spectra for the starting $Na_2O \cdot 2SiO_2$ glass, and a sample of coexisting glass and Si-free yellowish material synthesized from $Na_2O \cdot 2SiO_2$ + 8.8 wt% S with 0.2 wt% Gd_2O_3 as described in Figure 14. The top spectrum is the same as the middle one, but with the vertical scale expanded by five times. Arrows denote positions expected for SiO_3S and SiO_2S_2 species. The solid circle denotes spinning side band.

because it is known that sodium silicate glasses become more hygroscopic with decreasing silica content. No paramagnetic impurities were added to these samples, because our recent studies have suggested that the addition of even a small amount of Gd_2O_3 (0.2 wt%) can cause undesirable peak broadening and signal loss (Xue and Kanzaki, 2004b). To evaluate at what

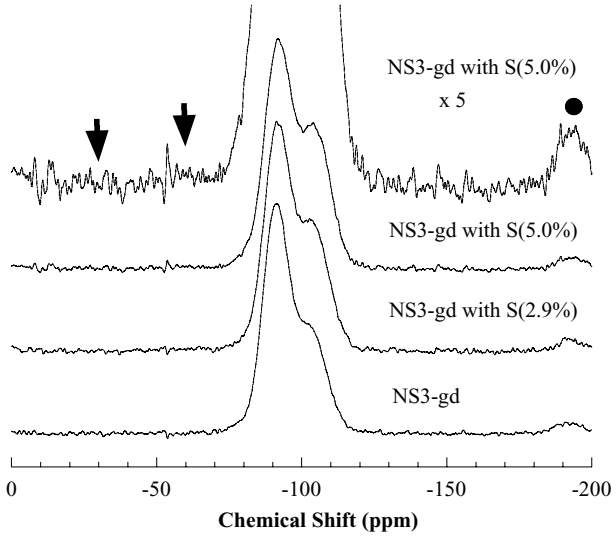

Fig. 6. ^{29}Si MAS NMR spectra for the starting $Na_2O \cdot 3SiO_2$ glass and samples synthesized from $Na_2O \cdot 3SiO_2$ + 2.9 and 5.0 wt% S and with 0.2 wt% Gd_2O_3. The top spectrum is the same as the one below, but with the vertical scale expanded by five times. Arrows denote positions expected for SiO_3S and SiO_2S_2 species. The solid circle denotes spinning side band. The sulfur-free glass was quenched from melt at 1200°C and ambient pressure, and the sulfur-bearing samples were quenched from melt + fluid at 1000°C and 1970 bar using the same batch of starting material, and consist of a homogeneous glass phase and a yellowish Si-free material condensed from the fluid.

stage water is incorporated into the sample, ^{1}H MAS NMR spectra have been taken on the starting $Na_2O \cdot 1.5SiO_2$ glass, and on the starting material mixtures of glass plus native sulfur or Na_2SO_4 immediately before loading and welding shut into Au capsule for high-pressure synthesis. The ^{1}H-NMR spectra for the synthesized samples were acquired shortly after the capsule was opened. For samples synthesized from native sulfur-doped starting materials, the yellowish material on the surface of the glass was still a liquid and left stains on the weighing paper during this procedure. A range of delay times between 5 and 120 s have been used to check the relaxation rate. A delay time of 40 s was found to be sufficient to obtain fully relaxed spectra for the starting $Na_2O \cdot 1.5SiO_2$ glass and the starting material mixtures containing native sulfur or Na_2SO_4, but a longer delay time of 80 s was necessary for sulfur-containing samples synthesized at high pressure.

In Figure 8 are plotted the ^{1}H MAS NMR spectra for the NS1.5e series of samples. The intensities for the plotted spectra have been normalized to sample weight and thus reflect the relative proton contents. The water content for the starting $Na_2O \cdot 1.5SiO_2$ glass (NS1.5e), estimated from the integrated area of the ^{1}H MAS NMR spectrum, is ~0.02 wt%, and those of the starting material mixtures of $Na_2O \cdot 1.5SiO_2$ glass plus Na_2SO_4 and $Na_2O \cdot 1.5SiO_2$ glass plus native sulfur are 0.03 and 0.1 wt%, respectively. The higher water content for the latter may reflect the fact that native sulfur could not be dried before usage, whereas the Na_2SO_4 powder was dried at 300°C. Samples recovered from high-pressure experiments contain significantly more water. The estimated water contents for the homogeneous glass samples synthesized from $Na_2O \cdot 1.5SiO_2$ plus 3 and 6 wt% Na_2SO_4 (e054 and e053) are both ~0.3 wt%; and those of the samples synthesized from $Na_2O \cdot 1.5SiO_2$ plus 3 and 6.7 wt% native sulfur (e052 and e051) are 0.6 and 1.8 wt%, respectively. Therefore, a significant amount of water was incorporated into the sample during high-pressure experiment. This may be, in part, related to the observed somewhat lower oxidation state of sulfur in the synthesized samples than in the starting materials. In another word, H_2 diffusing from the pressure medium of the IHPV apparatus could have reacted with the sample, producing H_2O and more reduced sulfur species.

The ^{1}H MAS NMR spectra also carry information about the water speciation in these samples. Although the incorporation of water into the sulfur-bearing silicate glasses complicates interpretations of changes in the silicate network structure, these data can be advantageously utilized to gain insight into the interaction of water with sulfur-bearing silicate melts, because water is often an important component in natural magmas. The ^{1}H MAS NMR spectrum of the starting $Na_2O \cdot 1.5SiO_2$ glass contains a broad peak in the range between ~2 to 17 ppm (Fig. 8a), similar to those of hydrous sodium silicate glasses (e.g., Kohn et al., 1989; Xue and Kanzaki, 2004b). Our recent ab initio calculations have suggested that intensities in the higher-frequency region (between ~8 and 17 ppm) reflect strongly hydrogen-bonded SiOH groups, and those in the lower-frequency region can be attributed to weakly to moderately hydrogen-bonded SiOH and molecular H_2O groups in the glass structure (see Xue and Kanzaki, 2004b). The ^{1}H MAS NMR spectra for both of the two homogeneous glass samples produced from $Na_2O \cdot 1.5SiO_2$ + Na_2SO_4 (e054 and e053) contain a broad, asymmetric peak in a similar range, and in

Table 3. Deconvolution results for Q^n species in glass samples from ^{29}Si MAS NMR.

	Q^2			Q^3			Q^4			
Sample[a]	Chemical shift (ppm)	FWHM (ppm)	%	Chemical shift (ppm)	FWHM (ppm)	%	Chemical shift (ppm)	FWHM (ppm)	%	NBO/T[b]
NS1.5a-gd	−76.9 (0.0)	6.2 (0.0)	27.7 (0.4)	−87.1 (0.1)	10.5 (0.1)	72.3 (0.4)				1.277 (0.004)
a501 (S = 1.4 wt%)	−76.8 (0.1)	6.1 (0.1)	18.4 (0.5)	−87.5 (0.1)	10.2 (0.1)	81.6 (0.5)				1.184 (0.005)
NS1.5b-gd	−76.8 (0.0)	6.2 (0.1)	27.8 (0.9)	−87.1 (0.1)	10.3 (0.1)	72.2 (0.9)				1.278 (0.009)
e002	−76.7 (0.1)	6.0 (0.1)	26.1 (0.6)	−87.1 (0.1)	10.4 (0.1)	73.9 (0.7)				1.261 (0.006)
e003 (S = 0.5 wt%)	−76.9 (0.0)	6.1 (0.1)	24.0 (0.5)	−87.3 (0.0)	10.5 (0.1)	76.0 (0.5)				1.240 (0.004)
NS2a-gd	−77.3 (0.1)	7.2 (0.3)	9.1 (0.7)	−88.4 (0.1)	9.9 (0.1)	79.1 (1.0)	−99.0 (0.5)	12.9 (0.5)[c]	11.8 (0.9)	0.973 (0.014)
d057 (S = 1.1 wt%)				−90.0 (0.0)	10.8 (0.1)	78.4 (1.2)	−102.2 (0.2)	12.0 (0.4)	21.6 (1.1)	0.784 (0.014)
NS2.3-gd	−77.7 (0.1)	6.5 (0.4)	4.6 (0.8)	−89.2 (0.1)	9.8 (0.0)	76.7 (0.8)	−100.0 (0.1)	12.9 (0.4)	18.6 (0.2)	0.858 (0.007)
b301 (S = 0.9 wt%)	−79.0 (0.1)	5.4 (0.2)	1.4 (0.3)	−89.7 (0.1)	10.0 (0.1)	69.9 (1.7)	−100.5 (0.2)	14.7 (0.5)	28.8 (1.8)	0.727 (0.022)
NS3-gd				−90.9 (0.0)	10.5 (0.0)	66.5 (0.5)	−103.2 (0.0)	12.4 (0.1)	33.5 (0.6)	0.665 (0.006)
tr030 (S = 0.7 wt%)				−91.8 (0.0)	11.1 (0.0)	60.5 (0.2)	−104.7 (0.0)	12.3 (0.0)	39.5 (0.2)	0.605 (0.002)
tr031 (S = 0.6 wt%)				−91.4 (0.0)	10.6 (0.1)	60.2 (1.0)	−103.9 (0.0)	12.9 (0.1)	39.8 (1.0)	0.602 (0.008)
NS1.5c-gd	−76.7 (0.1)	6.7 (0.1)	27.5 (0.2)	−87.0 (0.1)	10.9 (0.1)	72.5 (0.2)				1.275 (0.002)
e024 (S = 0.5 wt%)	−76.7 (0.1)	7.1 (0.3)	30.6 (0.2)	−86.7 (0.1)	10.4 (0.1)	69.4 (0.2)				1.301 (0.002)
e025 (S = 0.5 wt%)	−76.7 (0.1)	6.7 (0.3)	29.9 (0.2)	−86.7 (0.1)	10.3 (0.0)	70.1 (0.2)				1.299 (0.002)
e026 (S = 1.2 wt%)	−76.7 (0.1)	6.6 (0.2)	31.8 (0.3)	−86.6 (0.1)	10.4 (0.2)	68.2 (0.3)				1.318 (0.002)
NS2b-gd	−76.9 (0.1)	7.1 (0.2)	6.8 (0.4)	−88.7 (0.1)	9.9 (0.1)	83.6 (0.7)	−101.1 (0.3)	12.9 (0.5)[c]	9.5 (0.7)	0.973 (0.007)
d035 (S = 0.2 wt%)	−76.9 (0.1)	6.4 (0.2)	5.8 (0.5)	−88.5 (0.1)	9.5 (0.0)	86.7 (0.7)	−101.3 (0.3)	12.9 (0.5)[c]	7.5 (0.8)	0.983 (0.010)
d036 (S = 1.1 wt%)	−76.7 (0.1)	7.0 (0.2)	5.8 (0.5)	−88.5 (0.1)	9.5 (0.1)	87.6 (0.8)	−101.6 (0.4)	12.9 (0.5)[c]	6.6 (0.8)	0.991 (0.010)
d038 (S = 1.8 wt%)	−76.8 (0.1)	7.2 (0.1)	6.8 (0.4)	−88.4 (0.1)	9.7 (0.0)	86.2 (0.8)	−100.4 (0.5)	12.9 (0.5)[c]	7.0 (0.8)	0.998 (0.009)

[a] The sulfur contents labeled are those analyzed for the glasses using an electron microprobe.
[b] Calculated from Q^n speciation distribution.
[c] Value fixed during deconvolution.

Table 4. Raman data for various sulfur compounds and ions from the literature.[a]

	Raman peak (cm^{-1})	Reference[b]
SO_4^{2-} sol	451s, 613, 981s, 1104	1
SO_4^{2-} (Na_2SO_4) cry	450w, 470w, 620w, 630w, 645w, 994s, 1100w, 1130w, 1150w	2
$S_2O_7^{2-}$ ($Na_2S_2O_7$) cry	330, 347, 358, 520, 560, 586, 750, 1052, 1110, 1244, 1290	3
SO_3^{2-} sol	470, 620, 933, 966s	1
SO_3^{2-} (Na_2SO_3) cry	500m, 642w, 952m, 990s	4
$S_2O_3^{2-}$ sol	339, 451s, 541, 672, 1002, 1125	1
$S_2O_3^{2-}$ ($Na_2S_2O_3 \cdot 5H_2O$) cry	321w, 345w, 432s, 545w, 672w, 1015m, 1115m, 1162w	4
$S_2O_4^{2-}$ sol	232s, 461s, 584, 997, 1052	1
$S_2O_4^{2-}$ ($Na_2S_2O_4$) cry	132m, 177m, 252s, 359s, 1027m, 1040w, 1064w	4
$S_2O_5^{2-}$ sol	235s, 424s, 655s, 1052s	1
$S_2O_5^{2-}$ ($Na_2S_2O_5$) cry	200m, 225m, 273s, 317m, 429s, 512w, 530w, 552w, 655s, 974w, 1059s, 1083w, 1175w, 1198w	2
$S_2O_6^{2-}$ sol	281s, 320, 550, 710s, 1092s, 1206	1
$S_2O_6^{2-}$ ($Na_2S_2O_6 \cdot 2H_2O$) cry	292s, 333m, 541w, 555w, 706m, 1097s, 1215m	4
$S_4O_6^{2-}$ sol	148s, 260, 310, 390s, 522, 640, 1040s, 1230	1
S_2^- sol or cry	585–595s	5, 6
S_3^- sol or cry	535s, 233	5, 6
S_2^{2-} (β-Na_2S_2) cry	130w, 451s	7
S_3^{2-} (Na_2S_3) cry	458m, 476s	7
S_4^{2-} (Na_2S_4) cry	206w, 440w, 445s, 468w, 482m	7
S_4^{2-} (Na_2S_4) glass	446s, 476w, 487m	7
S_2^{2-} (Na_2S_s) cry	103w, 135w, 214w, 266w, 444s, 488w	7
S_5^{2-} (Na_2S_5) glass	410m, 444s, 480m	7
S_6^{2-} (K_2S_6) cry	254m, 337m, 358m, 373s, 453m, 495w, 504w	8
S_8 (elemental S) cry	154s, 218s, 456s, 472s	4
SiS_4^{4-} (edge-sharing) (SiS_2) cry	138m, 175m, 181m, 351m, 430s, 625w	9
SiS_4^{4-} (SiS_2) glass	121m, 174w, 367w, 381w, 427s, 625w,	9
SiS_4^{4-} (corner-sharing) ($Rb_4Si_4S_{10}$) cry	141s, 156s, 191vs, 264vs, 368s, 535w, 605w, 630m	10

[a] sol = in solution, cry = crystal, m = medium, s = strong, w = weak, vs = very strong.
[b] Reference: (1) Meyer et al. (1980); (2) Konijnendijk and Buster (1977); (3) Brown and Ross (1972); (4) Degen and Newman (1993); (5) Holzer et al. (1969); (6) Chivers and Lau (1982); (7) Janz et al. (1976b); (8) Janz et al. (1976a); (9) Tenhover et al. (1983); (10) Köster et al. (2002).

addition, a narrower peak near −2.3 ppm (see Fig. 8d, e). The broad peak may again have large contributions from hydrogen-bonded SiOH groups. However, it is known that within this region, the ^1H chemical shifts are dominated by the strength of hydrogen bonding, but are insensitive to the type of cations bonded to the OH groups (cf. Xue and Kanzaki, 2004b). For example, SOH (HSO_4^-) groups in alkali sulfate hydrates, tend to form strong hydrogen bonding and yield ^1H chemical shifts in a similar range (e.g., 12.7 to 14.6 ppm for the $KHSO_4$ phases, see Berglund and Vaughan, 1980; Kemnitz et al., 1996; Xue and Kanzaki, 2004b). Thus, either hydrogen-bonded SiOH, or SOH groups, or more likely both, may contribute to the intensities in the 2 to 17 ppm region. The partially resolved shoulder near 5 ppm could be attributed at least in part to molecular H_2O (also see discussions below). The sharp peak near −2.3 ppm is indicative of non-hydrogen-bonded OH groups, and cannot possibly be attributed to SiOH or SOH groups from comparison with experimental data and ab initio calculations (see Xue and Kanzaki, 2004b for discussions). On the other hand, it is well known that HS groups (protons linked to anionic sulfur species, such as HS^- or HS_x^-) in general do not form hydrogen bonding with other anions, because of the low electronegativity of sulfur. Our ab initio calculations on small clusters (Xue, unpublished data) have confirmed that HS groups yield small ^1H chemical shifts. In addition, we have found that a commercial high-purity crystalline Na_2S powder yields a sharp ^1H-NMR peak near this position that may be attributed to hydrated species on the surface. Thus, the most plausible assignment of the peak near −2.3 ppm is to HS groups. This represents another evidence for the presence of reduced sulfur species in glasses produced from Na_2SO_4-doped starting materials. The presence of the HS group (HS^-) has been suggested in previous sulfur solubility models for hydrous silicate melts under reduced conditions (e.g., Burnham, 1979). A small, sharp peak near 1.5 ppm is also seen in all the ^1H MAS NMR spectra and could be due to minor organic contaminations (Fig. 8).

The ^1H MAS NMR spectra for samples synthesized from $Na_2O \cdot 1.5SiO_2$ plus native sulfur contain contributions from both the glass and the coexisting yellowish material. The spectra for the two samples produced from $Na_2O \cdot 1.5SiO_2$ plus 3 and 6.7 wt% S (e052, e051) contain a broad peak in the 2 to 17 ppm range and a narrower peak near −2.3 ppm (see Fig. 8f, g), similar to those produced from Na_2SO_4-doped starting materials. In addition, there is a very prominent, sharp peak near 4.8 ppm with a FWHM of 0.16 ppm, similar to liquid water. This peak has a much shorter ^1H T_1 than the other peaks, and its intensity decreases markedly with time during NMR experiments at a spinning rate of 10 kHz. These features suggest that the sharp peak near 4.8 ppm is from mobile molecular H_2O that was gradually lost during sample spinning. Considering that these samples contained a liquid phase, in addition to the glass, at the start of the NMR experiment, it is likely that most of the mobile water resided in the liquid phase, rather than in the glass. The ^1H T_1 for the broad peak between 2 to 17 ppm and the narrower peak near −2.3 ppm are similar to each other, and to those of similar peaks in the homogeneous glass samples synthesized from Na_2SO_4-doped starting materials, and may thus be largely from the glass. The relative intensity of the −2.3 ppm peak to that of the broad, higher-frequency peak is

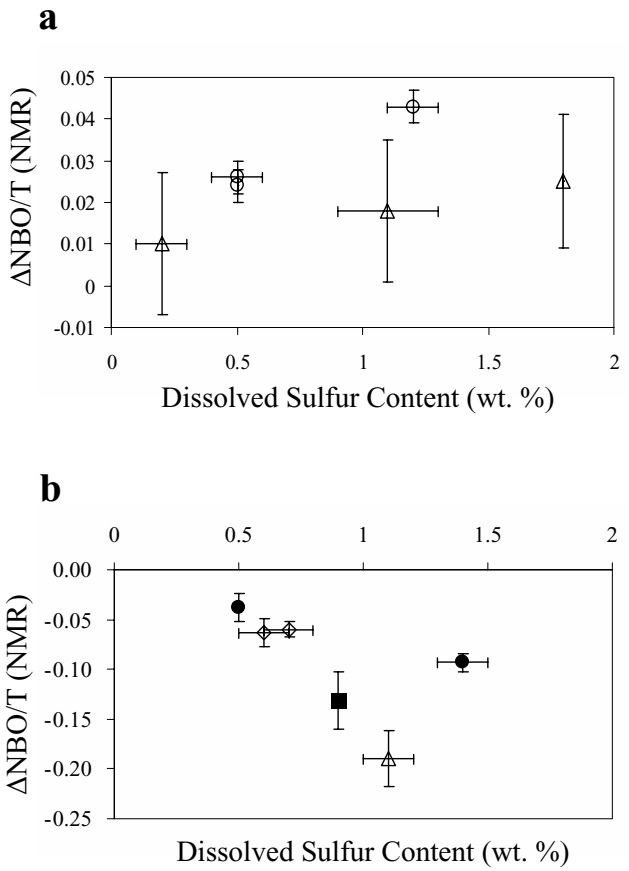

Fig. 7. Change in the degree of polymerization (ΔNBO/Si) between the sulfur-bearing glasses and starting glass estimated from ^{29}Si MAS NMR spectra, as a function of the added sulfur content (wt%) for samples synthesized from (a) $Na_2O \cdot xSiO_2 + Na_2SO_4$ and (b) $Na_2O \cdot xSiO_2$ + S. Circle: x = 1.5; triangle: x = 2; square: x = 2.3: diamond: x = 3; solid symbol: graphite-containing; open symbol: graphite-free.

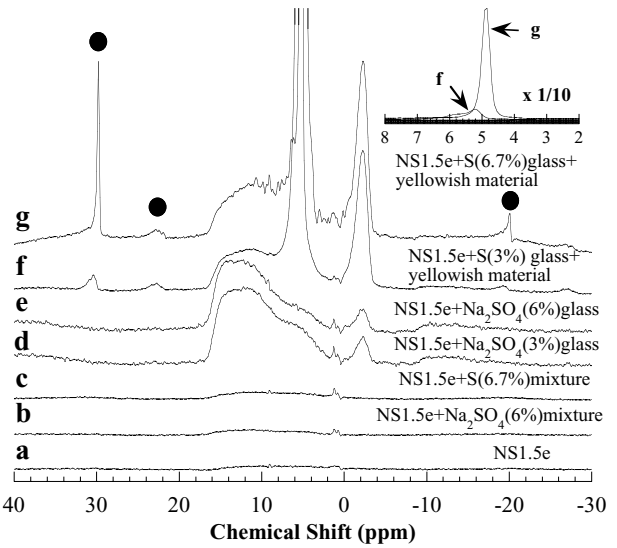

Fig. 8. ^{1}H MAS NMR spectra for (a) the starting $Na_2O \cdot 1.5SiO_2$ glass, (b) and (c) mixtures of $Na_2O \cdot 1.5SiO_2 + Na_2SO_4$ or S before high-pressure synthesis, (d) and (e) sulfur-bearing glasses synthesized from mixtures of $Na_2O \cdot 1.5SiO_2 + Na_2SO_4$, and (f) and (g) sulfur-bearing glasses coexisting with a yellowish material, synthesized from mixtures of $Na_2O \cdot 1.5SiO_2$ + S. The inset shows plots of the same spectra with expanded horizontal scale and reduced vertical scale (by 1/10), showing the sharp peak near 4.8 ppm, now only visible in (f) and (g). The starting $Na_2O \cdot 1.5SiO_2$ glass was quenched from melt at 1200°C and ambient pressure, and the sulfur-bearing samples were synthesized from melt (or melt-fluid) at 1000°C and 1970 bar. Sold circles denote spinning side bands.

much larger in these spectra than those of glasses prepared from Na_2SO_4-doped starting materials, consistent with greater abundance of reduced sulfur species. We have also obtained ^{1}H MAS NMR spectra for some of the samples synthesized from native sulfur-doped $Na_2O \cdot 2SiO_2$ and $Na_2O \cdot 3SiO_2$ starting materials (d057, tr030, tr031) (not shown). The general features of these spectra are similar to those of the samples synthesized from $Na_2O \cdot 1.5SiO_2$ + S described above.

We have also acquired ^{23}Na MAS NMR spectra for these samples. As was also shown by previous studies (e.g., Xue and Stebbins, 1993), the ^{23}Na NMR spectra of sodium silicate glasses are in general broad, and show only small changes with composition (see Fig. 9c, e for examples). The ^{23}Na MAS NMR spectra for the homogeneous glass samples produced from $Na_2O \cdot xSiO_2 + Na_2SO_4$ (not shown) are similar to those of the sulfur-free starting glasses. The ^{23}Na MAS NMR spectra for samples synthesized from native sulfur-doped starting materials could have contributions from both the glass and the coexisting yellowish material, when the latter also contains Na. These spectra have been acquired either after the ^{1}H MAS NMR measurements on samples freshly from opened capsules (e051, e052, d057), or some time after recovery from the capsule when the yellowish material had already solidified (tr030, tr031). The yellowish material in all the samples had solidified by the time the samples were recovered at the end of NMR measurements, so there is some ambiguity as to whether this material was already solidified at the time of ^{23}Na MAS NMR experiment for samples of the former (e051, e052, d057). The ^{23}Na MAS NMR spectra for the two samples synthesized from $Na_2O \cdot 1.5SiO_2$ plus 3 and 6.7 wt% native sulfur (e051, e052) both contain a broad, asymmetric peak similar to that of the sulfur-free starting glass (Fig. 9a, b). The ^{23}Na MAS NMR spectrum of a sample synthesized from $Na_2O \cdot 2SiO_2$ plus 8.8 wt% native sulfur (d057) contains a prominent, sharp peak near 1.5 ppm, and smaller sharp peaks near 17.7, 20, 24, and 30 ppm, on top of a broad, asymmetric peak (Fig. 9d). A much weaker, sharp peak near 1.5 ppm is also observed in the ^{23}Na MAS NMR spectra of samples synthesized from $Na_2O \cdot 3SiO_2$ plus 2.9 and 5.0 wt% native sulfur (tr031, tr030) (see Fig. 9g, f). These sharp peaks are most likely from crystalline or mobile sodium-containing phases in the yellowish material, consistent with the detection of Na in this material from qualitative electron microprobe analysis.

3.3. Raman Spectra and Their Interpretations

3.3.1. Na_2O-SiO_2 Starting Glasses

The Raman spectra for the sulfur-free $Na_2O \cdot xSiO_2$ glasses with and without 0.2 wt% Gd_2O_3 compositions are shown in Figure 10 to 15. The spectra in each of the figures are for the starting materials of the particular series of experiments. The

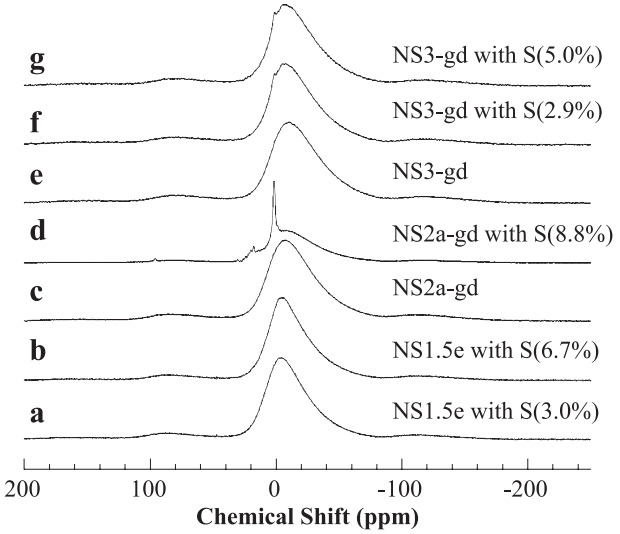

Fig. 9. ^{23}Na MAS NMR spectra for (a) and (b) samples synthesized from $Na_2O \cdot 1.5SiO_2$ + 3.0 and 6.7 wt% S with 0.2 wt% Gd_2O_3 (e052, e051), (c) the $Na_2O \cdot 2SiO_2$ starting glass with 0.2 wt% Gd_2O_3 (NS2a-gd), (d) a sample synthesized from $Na_2O \cdot 2SiO_2$ (NS2a-gd) + 8.8 wt% S (d057), (e) the $Na_2O \cdot 3SiO_2$ starting glass with 0.2 wt% Gd_2O_3 (NS3-gd), and (f) and (g) samples synthesized from $Na_2O \cdot 3SiO_2$ (NS3-gd) + 2.9 and 5.0 wt% S (tr031, tr030). All the samples synthesized from native sulfur-bearing starting materials contain a homogeneous glass phase, coexisting with a yellowish material condensed from the fluid.

spectra for a given composition are similar to one another and to those reported previously. The band assignments for these spectra are largely understood from extensive past studies (e.g., Brawer and White, 1975; Furukawa et al., 1981; Mysen et al., 1982; Matson et al., 1983; Fukumi et al., 1990; Xue et al., 1991; Mysen and Frantz, 1992, 1994): There is a strong high-frequency band near 1090 cm^{-1} that can be attributed to the symmetric Si-O stretching vibration of Q^3 species within the glass, and a weaker band near 950 cm^{-1} that grows in intensity with increasing Na_2O content and can be attributed the Si-O stretching vibration of Q^2 species. The Raman band in the 700−800 cm^{-1} region may correspond to motions of Si against its tetrahedral oxygen cage. Raman bands in the 500 ~ 600 cm^{-1} region can be attributed to Si-O-Si deformation vibration, coupled with tetrahedral O-Si-O bending vibrations. There is a high-frequency shoulder near 600 cm^{-1} on the main peak near 560 to 590 cm^{-1}. This shoulder has often been attributed to symmetric oxygen breathing vibration of three-membered siloxane rings (e.g., Matson et al., 1983; McMillan and Wolf, 1995).

Below, we first describe the Raman spectra for sulfur-bearing glasses synthesized from different starting materials (sections 3.3.2. to 3.3.3.), and then discuss the assignment of new bands in these spectra, paying particular attention to systematic changes with composition (section 3.3.4.).

3.3.2. *Glasses Synthesized from $Na_2O \cdot xSiO_2$ Plus Sodium Sulfate, Sulfite or Thiosulfate*

The Raman spectra for the homogeneous glass samples produced from $Na_2O \cdot xSiO_2 + Na_2SO_4$ (x = 1.5, 2), with and without 0.2 wt% Gd_2O_3, are shown in Figure 10 and 11. Both series of glasses show similar spectral changes. Within the high-frequency region, the most notable change is the appearance of a relatively narrow, new Raman band near 990 cm^{-1} for the sulfur-bearing glasses; the intensity of this band increases systematically with increasing added Na_2SO_4 content. In comparison, the relative intensity of the band near 950 cm^{-1} to that near 1090 cm^{-1} exhibits much smaller changes. Deconvolution of the high-frequency region with four gaussian peaks, one for each of the bands near 950 and 990 cm^{-1}, and two (near 1030 and 1080 cm^{-1}) for the asymmetric higher-fre-

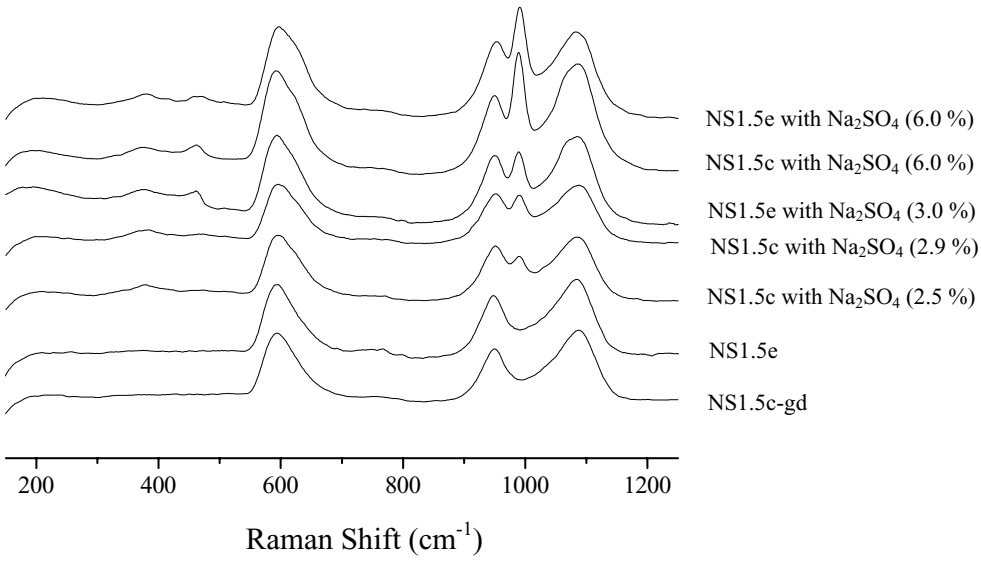

Fig. 10. Unpolarized Raman spectra for the starting $Na_2O \cdot 1.5SiO_2$ glasses and sulfur-bearing glasses synthesized from $Na_2O \cdot 1.5SiO_2 + Na_2SO_4$ with or without 0.2 wt% Gd_2O_3. The sulfur-free glasses were quenched from melt at 1200°C and ambient pressure, and the sulfur-bearing glasses were quenched from melts at 1000°C and 1970 bar. The labeled value in brackets is the added Na_2SO_4 content (wt%) in the starting material.

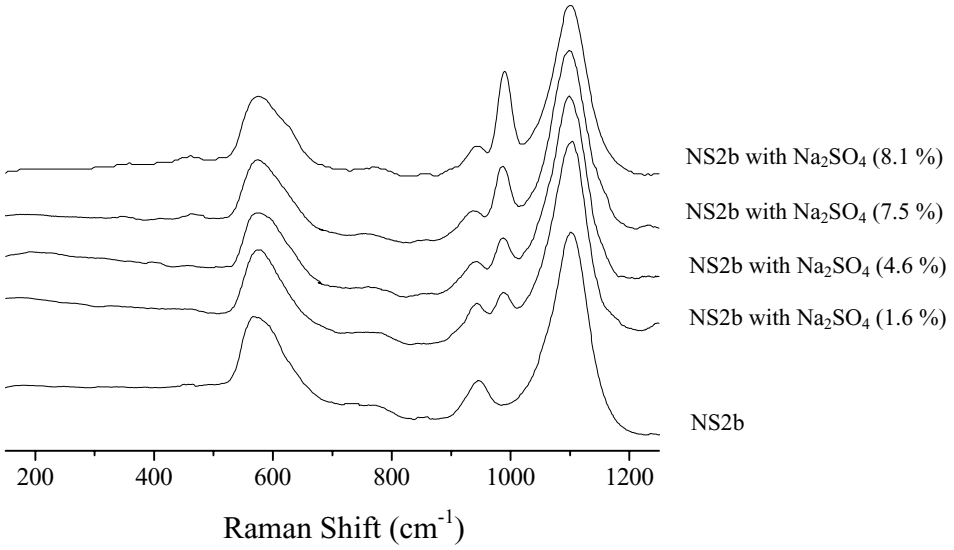

Fig. 11. Unpolarized Raman spectra for the starting $Na_2O \cdot 2SiO_2$ glasses and sulfur-bearing glasses synthesized from $Na_2O \cdot 2SiO_2 + Na_2SO_4$ with 0.2 wt% Gd_2O_3, also used in the NMR study (see Fig. 3).

quency band suggests that the intensity ratio between the band near 950 cm^{-1} and the asymmetric band near 1090 cm^{-1} increases slightly with sulfur content for the $Na_2O \cdot 1.5SiO_2$ series, but does not show discernible changes, partly due to small intensities, for the $Na_2O \cdot 2SiO_2$ series. Within the low-frequency region, weak new bands near 380 and 460 cm^{-1} appear and increase in intensity with increasing added Na_2SO_4 content for the $Na_2O \cdot 1.5SiO_2$ series (Fig. 10). Although weaker, these bands may also be present in the spectra for glasses synthesized from $Na_2O \cdot 2SiO_2 + Na_2SO_4$ (Fig. 11). The band near 590 cm^{-1} of the starting glasses apparently shifts to higher frequency with increasing added Na_2SO_4 content, due to the growth of a component near 620 cm^{-1} on its high-frequency shoulder.

The Raman spectra for the homogeneous glass samples synthesized from $Na_2O \cdot 1.5SiO_2 + Na_2SO_3$ and $Na_2O \cdot 1.5SiO_2 + Na_2S_2O_3$ are shown in Figure 12. These spectra resemble those for glasses synthesized from $Na_2O \cdot 1.5SiO_2 + Na_2SO_4$. A strong, relatively narrow band near 990 cm^{-1} in the high-frequency region, and two broader bands near 370 and 470 cm^{-1} in the low-frequency region are developed. The relative intensities of the two low-frequency bands are much larger than those of glasses synthesized from starting materials containing Na_2SO_4.

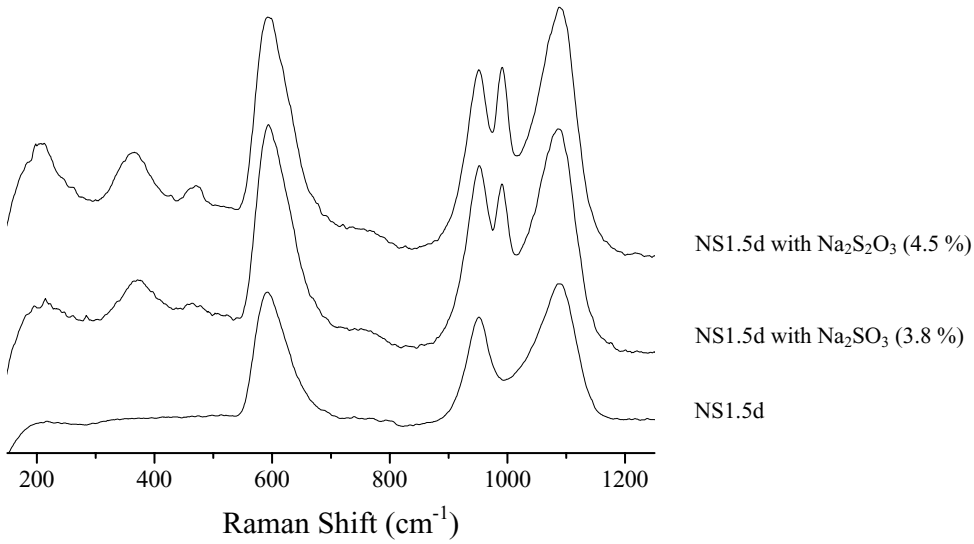

Fig. 12. Unpolarized Raman spectra for the starting $Na_2O \cdot 1.5SiO_2$ glass and sulfur-bearing glasses synthesized from $Na_2O \cdot 1.5SiO_2 + 3.8$ wt% Na_2SO_3 or 4.5 wt% $Na_2S_2O_3$. The starting glass was quenched from melt at 1200°C and ambient pressure, and the sulfur-bearing glasses were quenched from melts at 1000°C and 1970 bar using the same batch of starting glass.

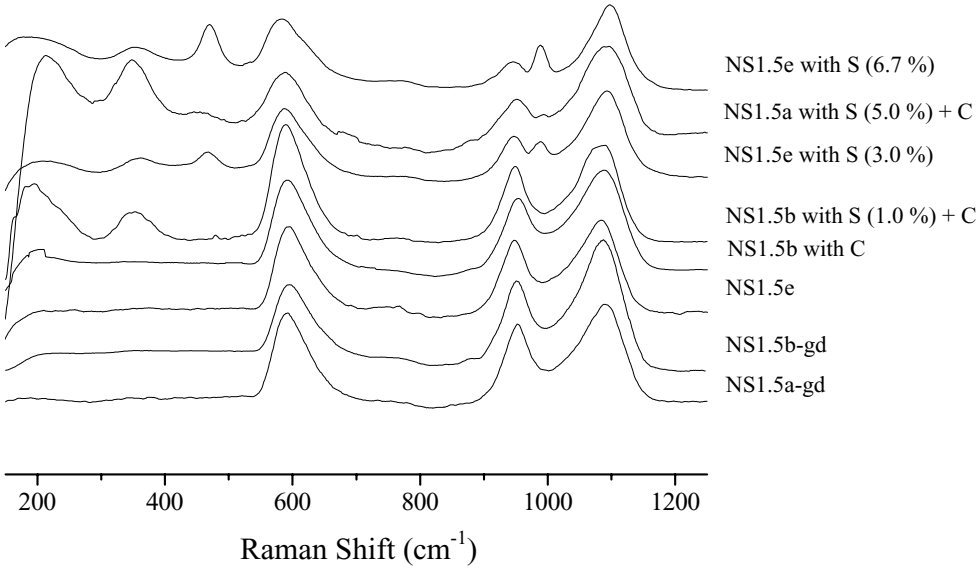

Fig. 13. Unpolarized Raman spectra for the starting $Na_2O \cdot 1.5SiO_2$ glasses and sulfur-bearing glasses synthesized from $Na_2O \cdot 1.5SiO_2$ + S with or without graphite and 0.2 wt% Gd_2O_3. Three batches of starting glasses (NS1.5a-gd, NS1.5b-gd and NS1.5e), all quenched from melts at 1200°C and ambient pressure, were used. The sulfur-bearing glasses were quenched from melts at 1000°C and 990 or 1970 bar, and coexist with a yellowish material condensed from the fluid. The labeled value in brackets is the added sulfur content (wt%) in the starting material.

3.3.3. Samples Synthesized from $Na_2O \cdot xSiO_2$ (x = 1.5, 2, 3) Plus Native Sulfur

For samples synthesized from native sulfur-doped $Na_2O \cdot xSiO_2$ (x = 1.5, 2, 3) starting materials, Raman spectra for the glass and for the coexisting, solidified yellow material have been acquired separately. The Raman spectra for the glasses in these samples are shown in Figure 13 to 15. In the high-frequency region, there is a systematic decrease in the relative intensity of the band near 950 cm^{-1} relative to that near 1090 cm^{-1} with increasing dissolved sulfur content, consistent with a decrease in the relative abundance of Q^2 to Q^3. In addition, a new, narrower peak near 990 cm^{-1} becomes clearly resolvable for glasses prepared from starting materials containing more than ~3 wt% sulfur. This peak is more prominent for glasses synthesized from $Na_2O \cdot 1.5SiO_2$ + S without graphite than those with graphite. In the low-frequency region, two new,

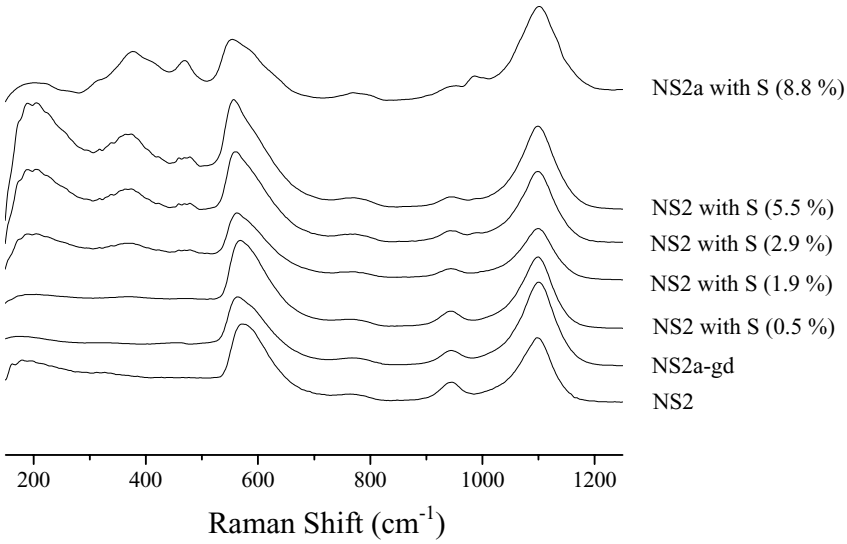

Fig. 14. Unpolarized Raman spectra for the starting $Na_2O \cdot 2SiO_2$ glasses and sulfur-bearing glasses synthesized from $Na_2O \cdot 2SiO_2$ + S with or without 0.2 wt% Gd_2O_3. Two batches of starting glasses (NS2 and NS2a-gd), both quenched from melt at 1200°C and ambient pressure, were used. The sulfur-bearing glasses were quenched from melts at 1000°C and 960–990 or 1970 bar and coexist with a yellowish material condensed from the fluid. The labeled value in brackets is the added sulfur content (wt%) in the starting material.

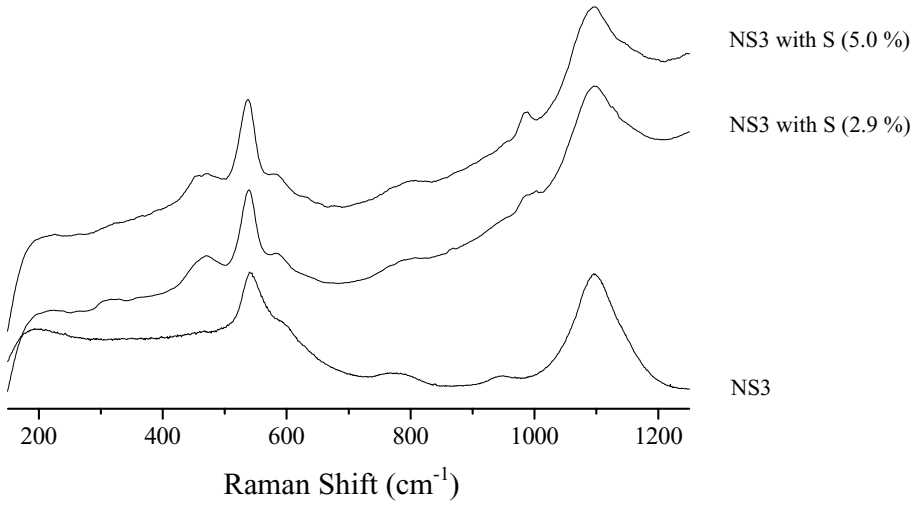

Fig. 15. Unpolarized Raman spectra for the starting $Na_2O \cdot 3SiO_2$ glass and sulfur-bearing glasses synthesized from $Na_2O \cdot 3SiO_2$ + 2.9 and 5.0 wt% S with 0.2 wt% Gd_2O_3, also used in the NMR study (see Fig. 6).

broad bands near 350 and 460 cm^{-1} appear in the spectra for glasses synthesized from $Na_2O \cdot 1.5SiO_2$ + S, with the former more prominent in graphite-doped samples and the latter stronger in the graphite-free samples (Fig. 13). Similar bands are also observed in the spectra of glasses synthesized from $Na_2O \cdot 2SiO_2$ + S, with the band near 350 cm^{-1} stronger than the 460 cm^{-1} band (Fig. 14). In the spectra for glasses synthesized from $Na_2O \cdot 3SiO_2$ + S, only the 460 cm^{-1} band is clearly visible (Fig. 15).

Representative Raman spectra for the solidified yellowish materials on the surface of glasses in some of these samples are shown in Figure 16. These spectra differ from those of the glasses in the same samples shown in Figure 13 to 15, either containing much sharper bands, or lacking high-frequency Raman bands characteristic of Si-O vibrations. Thus, the new

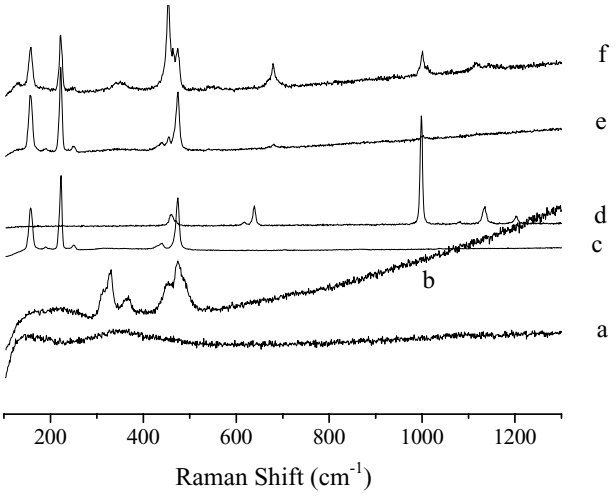

Fig. 16. Unpolarized Raman spectra for different parts of the solidified yellowish material adhered on the surface of glasses in samples synthesized from (a) $Na_2O \cdot 1.5SiO_2$ + 6.7 wt% S (e051), (b, c, d) $Na_2O \cdot 2SiO_2$ + 5.5 wt% S (d011), and (e, f) $Na_2O \cdot 3SiO_2$ + 5.0 wt% S (tr030).

bands described above for the Raman spectra of glasses in these samples are unlikely to be due to the presence of the yellowish material within the beam area, but reflect the structure of the glasses. These spectra also revealed that the yellowish material is composed of more than one substances, which vary with the composition of the starting materials. The Raman spectra for different parts of the yellowish material in a sample synthesized from $Na_2O \cdot 1.5SiO_2$ plus 6.7 wt% native sulfur (e051) all consist of a broad band near 350 cm^{-1} (Fig. 16a), that may be attributed to reduced sulfur in an amorphous phase (see discussion in the next section). This is consistent with the lack of sharp peaks in the ^{23}Na NMR spectra of this sample. The yellowish material in a sample synthesized from $Na_2O \cdot 2SiO_2$ plus 5.5 wt% native sulfur (d011) is heterogeneous, and the Raman spectra taken for different parts of the material show at least three patterns (Fig. 16b, c and d). The spectrum of Figure 16b contains strong bands near 330, 368, 454 and 474 cm^{-1}, but no bands in the high-frequency region, resembling spectra for crystalline and amorphous polysulfides (see Table 4). The spectrum of Figure 16c contains sharp bands near 157, 223, 448 and 474 cm^{-1}, identical to that of native sulfur (see Table 4). The spectrum of Figure 16d contains a strong sharp band near 988 cm^{-1}, and weaker, but sharp bands near 460, 639, 1135 and 1202 cm^{-1}. These bands agree well with those of crystalline Na_2SO_4 (see Table 4). Yellowish material giving the spectrum of Figure 16b, presumably polysulfides, is the most abundant in this sample and in two similar samples produced from starting materials with smaller amounts of native sulfur (d007, d009). Thus, these data are consistent with the presence of both S and Na in the solidified yellowish material in samples synthesized from native sulfur-doped $Na_2O \cdot 2SiO_2$, as revealed by electron microprobe analysis and supported by ^{23}Na NMR result for a similar sample (d057). The spectra for different parts of the yellowish material in a sample synthesized from $Na_2O \cdot 3SiO_2$ plus 5.0 wt% native sulfur (tr030) are shown in Figure 16e and f. These are similar to Figure 16c, and may be largely attributed to native sulfur. There is an additional strong band near 453 cm^{-1} and weaker bands near 679 and

1001 cm^{-1} in Figure 16f, which may be attributable to more oxidized sulfur species, possibly $Na_2S_2O_3$ (compare with Table 4). These results are consistent with the ^{23}Na NMR spectrum for this sample, which contains a small sharp peak attributable to a small amount of Na in the yellowish material. The oxidation states of the compounds observed in the yellowish material do not necessarily represent those of the fluid phase that coexisted with silicate melt during high-pressure experiment, because they were likely formed in contact with air after recovery from the metal capsule. Nevertheless, identification of these phases yields insight into the composition of the latter. The Raman, ^{23}Na NMR and electron microprobe analysis results altogether suggest that the fluid phase may contain S, Na and water, with their proportions depending on the bulk composition of the system.

3.3.4. *Band Assignment for the Raman Spectra of Sulfur-Bearing Glasses*

In this section, we discuss the assignment of the three new bands near 990, 350 ~ 380 and 460 cm^{-1} observed in the Raman spectra of sulfur-bearing glasses. The 990 cm^{-1} band is narrower than the 950 and 1095 cm^{-1} bands on either side due to Si-O stretching vibrations of Q^3 and Q^2 groups, and its intensity relative to those of the latter changes systematically with the concentration and oxidation state of dissolved sulfur in the glass. The other two peaks are within a region where no visible bands are observed for the sulfur-free $Na_2O \cdot xSiO_2$ glasses (x = 1,5, 2 and 3). Thus, all three bands are most likely related to dissolved sulfur species in the glass structure.

Extensive past experimental and theoretical studies on sulfur compounds and sulfur-containing solutions have shown that different sulfur groups tend to yield characteristic Raman bands that are similar in both crystalline phases and solutions (cf. Nakamoto, 1986) and may thus be expected to be similar in glasses, as well. Thus, band assignment can be made by comparing the spectra for sulfur-bearing glasses with those of crystalline phases and solutions. These data are compiled along with the respective references in Table 4. It is clear from these data that S-O stretching vibrations in general yield bands in the 900 to 1300 cm^{-1} region, whereas S-S and Si-S stretching and O-S-O bending vibrations tend to yield bands in the 200 to 600 cm^{-1} region.

We will first discuss band assignment for the most oxidized glasses of this study, synthesized from Na_2SO_4-doped $Na_2O \cdot xSiO_2$ (x = 1.5 and 2) (see Fig. 10, 11). The narrow band near 990 cm^{-1} grows systematically with sulfur content to become even more intense than bands on either side due to Si-O stretching vibrations. The other two new bands, near 380 and 460 cm^{-1}, though observable for the more sulfur-rich glasses, are much weaker. Because oxysulfur groups containing S-S linkages in general yield strong bands in the 200 to 600 cm^{-1} region (see Table 4 and the collection of Raman spectra in Degen and Newman, 1993), the weakness of the bands near 380 and 460 cm^{-1} relative to the 990 cm^{-1} band precludes the assignment of the latter to such groups. Oxysulfur species that do not contain S-S linkages include SO_4^{2-} (sulfate), SO_3^{2-} (sulfite), and polymerized species such as $S_2O_7^{2-}$. The last are rare in nature, and like polymerized silicate groups (Q^n with $n > 0$), they tend to yield larger S-O stretching frequencies than isolated species (e.g., 1110 cm^{-1} for crystalline $Na_2S_2O_7$: Brown and Ross, 1972; also see Table 4), and thus do not likely contribute to the observed band near 990 cm^{-1}. The SO_3^{2-} group is known to give two prominent bands, one near 970–990 cm^{-1} due to the symmetric S-O stretching and another near 950~970 cm^{-1} due to the asymmetric S-O stretching mode (e.g., Banister et al., 1968; Degen and Newman, 1993). Thus, the latter band, if present, may overlap with the band near 950 cm^{-1} for the Si-O stretching of Q^2 species. Nevertheless, because of the narrowness of the band near 990 cm^{-1}, if a companying second band were present, it is expected to be similarly narrow and may thus be at least partially resolvable from the latter. In addition, from the ^{29}Si-NMR results, the abundance ratio of Q^2/Q^3 for these glasses only varies slightly with increasing added Na_2SO_4. Thus, if such a second band accompanying the strong 990 cm^{-1} were indeed present, an apparent large increase in the relative intensity of the band due to Q^2 to Q^3 would be expected, and such an increase would be more prominent for the $Na_2O \cdot 2SiO_2$ series because the starting glass contains only a small amount of Q^2 species. The absence of a resolvable narrow component near 950~970 cm^{-1}, and the lack of significant increase in the intensity ratio of the 950 to 1090 cm^{-1} peak for both the $Na_2O \cdot 1.5SiO_2$ and the $Na_2O \cdot 2SiO_2$ series (Fig. 10, 11) preclude this possibility. On the other hand, these new bands match well with features for isolated SO_4^{2-} group. SO_4^{2-} groups in both crystalline sulfates and in solutions are known to yield the strongest peak near 990 cm^{-1} attributable to the symmetric S-O stretching mode, and in addition yield weak bands near 630 cm^{-1} attributable to the asymmetric O-S-O bending modes, weak bands near 470 cm^{-1} attributable to the asymmetric O-S-O bending modes, and weak bands near 1130 cm^{-1} attributable to the asymmetric S-O stretching modes (e.g., Konijnendijk and Buster, 1977, also see Table 4). The increase in intensity near 620 cm^{-1} and the appearance of a weak band near 460 cm^{-1} for the sulfur-bearing glasses (Fig. 5 and 6) could both be related to the presence of the SO_4^{2-} group. Konijnendijk and Buster (1977) also observed relatively narrow Raman bands near 460, 620 and 980 cm^{-1} for K_2O-SiO_2 glasses doped with K_2SO_4, and attributed all of them to dissolved K_2SO_4 species. McKeown et al. (2001) reported similar, narrow Raman bands for Na_2SO_4-doped borosilicate glasses and noted that the position of the band near 980 cm^{-1} moves systematically with the type of metal cations (Na, Li, K, Ca), parallel to the trend shown by crystalline sulfates. All these evidences are in supportive of the assignment of the major, relatively narrow band near 990 cm^{-1} and the weaker band near 450 cm^{-1} for these glasses to isolated SO_4^{2-} group. As pointed out previously (e.g., McKeown et al., 2001), the prominence of the band near 990 cm^{-1}, even at relatively low sulfur concentrations, can be related to the large Raman cross section of such group due to the greater polarizability of the S-O bonds than Si-O and B-O bonds. Considering that the average valence of sulfur in these glasses are somewhat more reduced than sulfate, as revealed by the SKα wavelength shift results, the remaining weak band near 350 ~ 380 cm^{-1} is most likely related to reduced sulfur species. The less conspicuous intensity near this position for the $Na_2O \cdot 2SiO_2$ series than for the $Na_2O \cdot 1.5SiO_2$ series are consistent with the higher average valence of the former as suggested by the SKα wavelength shifts. Such an assignment is

also supported by Raman spectra of more reduced sulfur-bearing glasses as discussed below.

Compared with the Raman spectra for glasses produced from Na_2SO_4-doped starting materials, the relative intensity of the broad band near 350 ~ 380 cm^{-1} becomes stronger, and that of the band near 980 cm^{-1} becomes much weaker in the spectra of more reduced glasses synthesized from Na_2SO_3-, $Na_2S_2O_3$- and native sulfur-doped $Na_2O \cdot 1.5SiO_2$ starting materials (see Fig. 10, 12, 13). There are no other obvious new bands growing in the high-frequency region for the latter glasses. Thus, it is likely that the band near 990 cm^{-1} in the more reduced glasses are also due to isolated SO_4^{2-} group. The greater intensity of the band near 350 ~ 380 cm^{-1} for these glasses is in agreement with its assignment to reduced sulfur species. The relative intensities of the 460 cm^{-1} band to that near 990 cm^{-1} for glasses produced from Na_2SO_3-, $Na_2S_2O_3$-, and Na_2SO_4-doped starting materials are similar (Fig. 10, 12) and may all be attributed to the SO_4^{2-} group, but those of more reduced glasses synthesized from native sulfur-doped $Na_2O \cdot 1.5SiO_2$ starting materials, especially samples without graphite, are much higher (Fig. 13). This suggests that the 460 cm^{-1} band in the latter must have additional contributions from more reduced sulfur species, besides the SO_4^{2-} group. Reduced sulfur species that yield strong Raman bands near these positions include those containing the Si-S and S-S linkages (see Table 4). The Si-S stretching modes of crystalline SiS_2 and $Rb_4Si_4S_{10}$, for example, are known to produce strong Raman bands near 430 and 368 cm^{-1}, respectively (e.g., Tenhover et al., 1983; Köster et al., 2002; also see Table 4). However, as described in section 3.2, our ^{29}Si-NMR spectra revealed no peaks attributable to $SiO_{4-n}S_n$ ($n > 0$) groups in any of the glasses synthesized from $Na_2O \cdot xSiO_2$ plus Na_2SO_4, Na_2SO_3, $Na_2S_2O_3$ and native sulfur. Especially for samples with larger dissolved sulfur concentrations, the lack of such NMR peaks suggests that the $SiO_{4-n}S_n$ groups, even if present, cannot contribute to the intensities near 350 ~ 380 and 460 cm^{-1} to any significant extent. More possible candidates for these bands are species containing S-S linkages. Sulfur species giving rise to strong S-S stretching vibration bands near 350 ~ 380 cm^{-1}, but weaker or no bands in the middle- and high-frequency region, include the $S_2O_4^{2-}$ ($[O_2S\text{-}SO_2]^{2-}$) (e.g., 359 cm^{-1} for $Na_2S_2O_4$: see Degen and Newman, 1993, also Table 4) and S_6^{2-} (polysulfide) (e.g., 337 to 373 cm^{-1} for crystalline K_2S_6: see Janz et al., 1976a and Table 4) groups. The band near 350 ~ 380 cm^{-1}, relative to that near 990 cm^{-1}, is the strongest for the most reduced glasses of the $Na_2O \cdot 1.5SiO_2$ series, synthesized from native sulfur- and graphite-doped starting materials (see Fig. 13). From the SKα wavelength shift information, these glasses have an average sulfur valence significantly below that of native sulfur (see section 3.1. and Table 2). Thus, the more reduced polysulfide, S_6^{2-} group, rather than $S_2O_4^{2-}$, can better account for the sulfur valence. The observation of a ^{1}H-NMR peak near −2.3 ppm attributable to HS groups in all the glasses including those synthesized from sulfate-doped starting materials (see section 3.2.2), is also consistent with the presence of anionic sulfur. Thus, the most likely assignment for the broad band near 350 ~ 380 cm^{-1} is the polysulfide, S_6^{2-} group. Hanada et al. (1976) have attributed the red or brown color in alkali silicate and alkali borate glasses to the formation of polysulfides. Almost all the sulfur-bearing glasses obtained in this study are red- or reddish yellow–colored, consistent with this interpretation. Sulfur species that give rise to strong S-S stretching vibration bands near 460 cm^{-1}, but weaker or no bands in the middle- and high-frequency region include polysulfides of various lengths (S_x^{2-} with x = 2 to 6), elemental sulfur (S_8) and thiosulfate ($S_2O_3^{2-}$) (see Table 4). Although the S_6^{2-} group, inferred from the band near 350 ~ 380 cm^{-1}, and other polysulfide groups could contribute to intensity near this position, it is likely that this band has contributions from additional sulfur species, such as polymeric sulfur and/or thiosulfate, that are more reduced than SO_4^{2-}, but more oxidized than S_6^{2-}, because its relative intensity with respect to the band near 350 ~ 380 cm^{-1} is higher in the absence of graphite for sulfur-bearing glasses synthesized from $Na_2O \cdot 1.5SiO_2$ + S (see Fig. 13).

Raman bands near 990, 350 ~ 380 and 460 cm^{-1} for glasses in the $Na_2O \cdot 2SiO_2$-S and $Na_2O \cdot 3SiO_2$-S series may be similarly attributed to sodium sulfate, polysulfide and possibly other sulfur species of intermediate valence. It is worth noting that although the average sulfur valences (SKα wavelength shifts) of glasses synthesized from $Na_2O \cdot 3SiO_2$ + S (−1.2 ~ 1.4 × 10^{-3} Å) and $Na_2O \cdot 1.5SiO_2$ + $Na_2S_2O_3$ (−1.3 × 10^{-3} Å) are similar, the relative intensities of the Raman bands near 990, 350 ~ 380 and 460 cm^{-1} are considerably different (compare Fig. 12 and 15). Thus, the distribution of these sulfur species likely depends on both the f_{O2} and Na/S ratio of the system.

In summary, the Raman spectra for the sulfur-bearing Na_2O-SiO_2 glasses change systematically with the content and valence state of sulfur, and suggest the coexistence of isolated sulfate (Na_2SO_4) species and one or more types of more reduced sulfur species containing S-S linkages. The Na_2SO_4 group is the dominant sulfur species in the more oxidized glasses produced from Na_2SO_4-doped starting materials, but is also present in smaller quantities in more reduced glasses. This group is most likely responsible for the relatively narrow Raman band near 990 cm^{-1}, and may also contribute partly to intensities near 620 cm^{-1} and 460 cm^{-1}. More reduced sulfur species, possibly the polysulfide S_6^{2-} group, which contribute to the broad Raman bands near 350 ~ 380 cm^{-1}, are predominant in the relatively reduced glasses synthesized from native sulfur- and graphite-doped starting materials, but are also present in smaller amounts in more oxidized glasses. Other polysulfide groups and sulfur species of intermediate oxidation state may also be present in glasses synthesized from native sulfur-doped starting materials, and may partially contribute to the Raman band near 460 cm^{-1}. The distribution of these sulfur species seems to be affected by both the f_{O2} and Na/S ratio of the system. It should be pointed out that we cannot preclude the possibility for the presence of other sulfur species, such as Na_2S, that are expected to give lower-frequency Raman bands than the studied frequency region (below 200 cm^{-1}) because of the weak Na-S bonds. Nevertheless, such possibility is probably low, considering that coexisting sulfur species of at least two different valence states are already identified.

3.4. Changes in the Silicate Network Structure of Sulfur-Bearing Glasses

The results from the preceding sections can be applied to interpret changes in the polymerization of silicate network for

the sulfur-bearing silicate glasses as revealed from ^{29}Si-NMR. Interpretations for glasses synthesized from Na_2SO_4-doped starting materials are relatively straightforward because of the homogeneous nature of these samples. The ^{29}Si-NMR results for these glasses suggest that changes in the network structure are subtle, with perhaps a slight increase in NBO/T for the sulfur-bearing glasses compared to those of the sulfur-free starting glasses. If all the added Na_2SO_4 were dissolved as Na_2SO_4 species, no net change in the polymerization of the silicate structure would be expected. The lack of significant change in polymerization is consistent with the presence of Na_2SO_4 species as the dominant sulfur species in the glass structure. The conversion of some of the added Na_2SO_4 to reduced species containing S-S linkages, such as polysulfide (Na_2S_x), in the melts as inferred from the Raman spectra would have the effect of depolymerizing the silicate network structure, because of the release of some of the Na_2O due to the smaller Na/S ratio of the latter. This effect can be described by the following reaction, in the case of polysulfide species:

$$xNa_2SO_4\ (melt) = Na_2S_X\ (melt) + (x - 1)Na_2O\ (melt) + (3x + 1)/2O_2(vapor) \quad (2)$$

Another possible cause for the apparent small increase in NBO/T of the sulfur-bearing glasses may be related to the dissolved water. As revealed by the ^{1}H-NMR, the water contents in the sulfur-bearing glasses are about one order of magnitude higher than those in the starting glasses, and the dissolved water are in the form of SiOH and/or SOH groups, HS groups and molecular H_2O. The formation of SiOH groups is known to have a major depolymerizing effect on the silicate network (cf. McMillan, 1994; Xue and Kanzaki, 2004b), through the following familiar reaction:

$$SiOSi\ (melt) + H_2O\ (melt) = 2SiOH\ (melt) \quad (3)$$

The formation of SOH and HS groups are similarly expected to have a depolymerizing effect. For example, the reaction of water with sulfate and polysulfide species may be expressed by the following cation exchange reactions between Na^+ and H^+:

$$2Na_2SO_4\ (melt) + H_2O\ (melt) = 2NaHSO_4\ (melt) + Na_2O\ (melt) \quad (4)$$

$$2Na_2S_x\ (melt) + H_2O\ (melt) = 2NaHS_x\ (melt) + Na_2O\ (melt) \quad (5)$$

The release of Na_2O to the silicate network in these reactions would cause depolymerization of the latter. Thus, both the formation of reduced sulfur species containing S-S linkages, such as polysulfides, and the dissolution of water in the melt may contribute to the observed small depolymerization.

Changes to the glass structure for samples produced from native sulfur-doped starting materials are more complicated. Because of the coexistence of a sulfur- and sodium-bearing phase, the silicate compositions (Na/Si ratio) of the glasses are different from those of the starting glasses. In addition, these glasses contain more water than the starting glasses. These factors must be taken into account before the effect of the dissolved sulfur on the silicate network structure can be evaluated. The estimated change in NBO/T between the sulfur-bearing glasses and the starting glasses, from the ^{29}Si MAS NMR spectra reflect the combined effect of all these factors. To isolate the effect of changes in the silicate composition (Na/Si ratio) from the rest, we have plotted in Figure 17 the difference in the estimated change in NBO/T from ^{29}Si MAS NMR and that from electron microprobe analysis, as a function of the dissolved sulfur content. For the estimation of change in the NBO/T from the latter, only the effect of changing Na/Si ratio is included, by treating all the sodium as network-modifiers, each converting one bridging oxygen to a nonbridging oxygen. This plot clearly shows that the large increase in polymerization for the sulfur-containing glasses, relative to the respective starting glasses, observed from ^{29}Si MAS NMR, is dominantly due to the changing Na/Si ratio of the melt as a result of partitioning of some of the sodium into the coexisting fluid phase. There may be a small residual decrease in NBO/T, though not clearly resolvable, for the sulfur-containing glasses, compared to the starting glasses, after the effect of changing Na/Si is removed (see Fig. 17). Other factors that may cause an increase in the polymerization of the silicate network are the formation of Na-containing sulfur species, such as Na_2SO_4 and Na_2S_x species, as inferred from the Raman spectra, from the added S, because their formation scavenges Na_2O from the silicate network. The formation of sulfate and polysulfide species in the melt structure from the added elemental sulfur under a constant f_{O2} condition may be expressed by the following disproportionation reaction:

$$(3x + 1)S^0\ (fluid) + 4Na_2O\ (melt) = 3Na_2S_x\ (melt) + Na_2SO_4\ (melt) \quad (6)$$

This reaction may be combined with reaction (2) to account for situations under varying f_{O2} conditions. The formation of other Na-containing sulfur species has similar effects and may be expressed in similar reactions. The dissolution of water, on the other hand, is expected to have an opposite effect on the network structure.

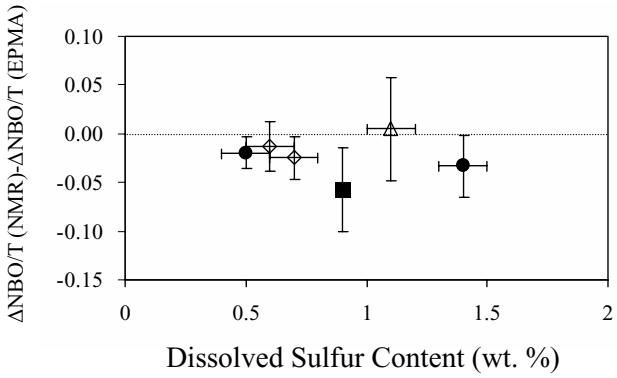

Fig. 17. Difference in the change of degree of polymerization (ΔNBO/T) estimated from ^{29}Si MAS NMR spectra and that from electron microprobe analyses, as a function of the dissolved sulfur content (wt%) for glasses synthesized from $Na_2O \cdot xSiO_2$ + S. Circle: x = 1.5; triangle: x = 2; square: x = 2.3: diamond: x = 3; solid symbol: graphite-containing; open symbol: graphite-free.

4. CONCLUSIONS

We have synthesized sulfur-bearing sodium silicate glasses (quenched melts) at 1000 to 1300°C and 1 to 2 kbar from starting materials containing sulfur of various valence states (Na_2SO_4, Na_2SO_3, $Na_2S_2O_3$ and S), and have investigated the sulfur speciation and the network structure of these glasses with electron-induced SKα X-ray fluorescence, micro-Raman and ^{29}Si, ^{1}H and ^{23}Na MAS NMR spectroscopic techniques. The following conclusions may be drawn:

(1) The average oxidation states of sulfur in these glasses, as revealed by the wavelength of the SKα X-rays, change systematically with the oxidation state of the sulfur compound added to the starting material, and are slightly lower than those of the added compounds for more oxidized samples. This suggests that the oxidation states of the synthesized glasses are largely dictated by sample compositions, with a small reduction for more oxidized starting materials. The sulfur-bearing silicate glasses contain more water than those of the starting glasses, possibly largely related to the small reduction of sulfur as a result of penetration of H_2 from the pressure medium during high-pressure synthesis. Thus, these samples may be better regarded as hydrous glasses and yield insight into the interaction between water and sulfur-bearing silicate melts.

(2) Whereas all the run products from sulfate-, sulfite-, and thiosulfate-doped starting materials are homogeneous glasses, those from native sulfur-doped starting materials are composed of a homogeneous glass coexisting with a material that contains sulfur, sodium and proton, but no silicon. The compositions of the latter must be within the silicate melt-fluid immiscibility region at the pressure and temperature condition of synthesis.

(3) The Raman spectra support the coexistence of Na_2SO_4 and one or more types of more reduced sulfur species containing S-S linkages in the structure of all the sulfur-bearing Na_2O-SiO_2 glasses. The former is dominant in glasses produced from the Na_2SO_4-doped starting materials, and the latter more abundant in more reduced glasses synthesized from native sulfur-doped starting materials. The ^{1}H-NMR data also revealed the coexistence of SiOH and/or SOH groups and HS group in these glasses, with the latter more abundant in the more reduced samples. We observed no detectable Si-S linkages from the ^{29}Si MAS NMR spectra of all the sulfur-bearing Na_2O-SiO_2 glasses, suggesting that sulfur preferentially coordinate with Na and O, rather than Si, in the studied system.

(4) The ^{29}Si MAS NMR and Raman data suggest that glasses synthesized from Na_2SO_4-doped starting materials show only small changes in the network structure, being slightly less polymerized than the starting glasses, whereas the structure of glasses produced from native sulfur-doped starting materials are significantly more polymerized than the starting glasses. The former can be accounted for by the dominant presence of sodium sulfate species with a small amount of more reduced sulfur species containing S-S linkages, possibly sodium polysulfide, and water species in the melt structure, and the latter may be the combined effect of (a) change in the Na/Si ratio of the melt due to the partitioning of Na into the coexisting fluid phase, (b) the presence sulfate and sodium-containing reduced sulfur species, such as sodium polysulfide, and (c) the incorporation of water in the melt structure.

It is highly likely that when the f_{O2} conditions and compositions of silicate melts are further varied, other sulfur species may come into play. In particular, at more reduced conditions, sulfide species, such as Na_2S and $SiO_{4-n}S_n$ groups, may become important. Further studies on silicate melts and glasses of a range of compositions and water contents under varying pressure, temperature, f_{O2} conditions are desirable for a better understanding of the behavior of sulfur in silicate melts/glasses and for direct application to natural magmatic systems.

Acknowledgments—We thank Dr. S. Yamashita for permission to use the IHPV apparatus and for constructive discussions. T.T. is grateful to Prof. E. Takahashi (Tokyo Inst. Tech.) for permission to use the IHPV apparatus at the early stage of this study and for instruction in the technique, to Prof. Y. Kudoh (Tohoku Univ.) and Dr. T. Kawamoto (Kyoto Univ.) for helpful advice, and to Profs. M. Kusakabe and H. Chiba for technical support of the ion chromatography. This manuscript has benefited from helpful comments by Dr. B. Mysen (associate editor), Dr. M.R. Carroll and two anonymous reviewers. This study was supported by Grants-in-Aid for Scientific Research to M.K. and 21st century COE Program from the Ministry of Education, Culture, Sports, Science and Technology of Japan.

Associate editor: B. Mysen

REFERENCES

Abraham K. P., Davies M. W., and Richardson F. D. (1960) Sulphide capacities of silicate melts, Part II. *J. Iron Steel Inst.* **196,** 309–312.

Ahmed A. A., El-Shamy T. M., and Sharaf N. A. (1980) States of sulfur in alkali borate glasses. *J. Am. Ceram. Soc.* **63,** 537–542.

Ahmed A. A., Sharaf N. A., and Condrate R. A. Sr. (1997) Raman microprobe investigation of sulphur-doped alkali borate glasses. *J. Non-Cryst. Solids.* **210,** 59–69.

Asahi T., Ino T., Miura Y., Nanba T., and Yamashita H. (1998) Chemical bonding state of sulfur in Na_2S-SiO_2 glasses. *J. Ceram. Soc. Japan.* **106,** 150–154.

Banister A. J., Moore L. F. and Padley J. S. (1968) Structural studies of sulphur species. In *Inorganic Sulphur Chemistry* (ed. G. Nickless), pp. 137–198. Elsevier.

Berglund B. and Vaughan R. W. (1980) Correlations between proton chemical shift tensors, deuterium quadrupole couplings and bond distances for hydrogen bonds in solids. *J. Chem. Phys.* **73,** 2037–2043.

Brawer S. A. and White W. B. (1975) Raman spectroscopic investigation of the structure of silicate glasses. 1. The binary alkali silicates. *J. Chem. Phys.* **63,** 2421–2432.

Brown R. G. and Ross S. D. (1972) The vibrational spectra of some condensed tetrahedral anions $[X_2O_7]^{n-}$. *Spectrochim. Acta* **28A,** 1263–1274.

Buchanan D. L. and Nolan J. (1979) Solubility of sulfur and sulfide immiscible in synthetic tholeiitic melts and their relevance to Bushveld-complex rocks. *Can. Min.* **17,** 483–494.

Burnham C. W. (1979) Magmas and hydrothermal fluids. In *Geochemistry of Ore Deposits*, Vol. 2 (ed. H. L. Barnes), pp. 71–136. Wiley.

Carroll M. R. and Rutherford M. J. (1985) Sulfide and sulfate saturation in hydrous silicate melts. *J. Geophys. Res.* **90,** C601–C612.

Carroll M. R. and Rutherford M. J. (1987) The stability of igneous anhydrite: Experimental results and implications for sulfur behavior in the 1982 El Chichon trachyandesite and other evolved magmas. *J. Petrol.* **28,** 781–801.

Carroll M. R. and Rutherford M. J. (1988) Sulfur speciation in hydrous experimental glasses of varying oxidation states: Results from measured wavelength shifts of sulfur X-rays. *Am. Min.* **73,** 845–849.

Chivers T. and Lau C. (1982) Raman spectroscopic identification of the S_4N^- and S_3^- ions in blue solutions of sulfur in liquid ammonia. *Inorg. Chem.* **21,** 453–455.

Cory D. G. and Ritchey W. M. (1988) Suppression of signals from the probe in Bloch decay spectra. *J. Magn. Reson.* **80,** 128–132.

Danckwerth P. A., Hess P. C., and Rutherford M. J. (1979) The solubilities of sulfur in high-TiO_2 mare basalts. In *Proceedings of the 10th Lunar Planetary Science Conference,* pp. 517–530. Lunar Planetary Science.

Degen I. A. and Newman G. A. (1993) Raman spectra of inorganic ions. *Spectrochim. Acta* **49,** 859–887.

Dupree R., Holland D., McMillan P. W., and Pettifer R. F. (1984) The structure of soda-silicate glasses: A MAS NMR study. *J. Non-Cryst. Solids* **68,** 399–410.

Fincham C. J. B. and Richardson F. D. (1954) The behavior of sulphur in silicate and aluminate melts. *Proc. R. Soc. Lond. A* **223,** 40–62.

Fukumi K., Hayakawa J., and Komiyama T. (1990) Intensity of Raman band in silicate glasses. *J. Non-Cryst. Solids* **119,** 297–302.

Furukawa T., Fox K. E., and White W. B. (1981) Raman spectroscopic investigation of the structure of silicate glasses. 2. Raman intensities and structural units in sodium silicate glasses. *J. Chem. Phys.* **75,** 3226–3237.

Gurenko A. A. and Schmincke H.-U. (2000) S concentrations and its speciation in Miocene basaltic magmas north and south of Gran Canaria (Canary Islands): Constraints from glass inclusions in olivine and clinopyroxene. *Geochim. Cosmochim. Acta* **64,** 2321–2337.

Haughton D. R., Roeder P. L., and Skinner B. J. (1974) Solubilities of sulfur in mafic magmas. *Econ. Geol.* **69,** 451–467.

Holzer W., Murphy W. F., and Bernstein H. J. (1969) Raman spectra of negative molecular ions doped in alkali halide crystals. *J. Mol. Spect.* **32,** 13–23.

Janz G. J., Coutts J. W., Downey J. R. Jr., and Roduner E. (1976a) Raman studies of sulfur-containing anions in inorganic polysulfides. Potassium polysulfides. *Inorg. Chem.* **15,** 1755–1759.

Janz G. J., Downey J. R. Jr., Roduner E., Wasilczyk G. J., Coutts J. W., and Eluard A. (1976b) Raman studies of sulfur-containing anions in inorganic polysulfides. Sodium polysulfides. *Inorg. Chem.* **15,** 1759–1763.

Katsura T. and Nagashima S. (1974) Solubility of sulfur in some magmas at atmosphere. *Geochim. Cosmochim. Acta* **38,** 517–531.

Kemnitz E., Werner C., and Trojanov S. I. (1996) Structural chemistry of alkaline metal hydrogen sulfates. A review of new structural data. Part II. Hydrogen-bonding systems. *Eur. J. Solid State Inorg. Chem.* **33,** 581–596.

Keppler H. (1999) Experimental evidence for the source of excess sulfur in explosive volcanic eruptions. *Science* **284,** 1652–1654.

Kirkpatrick R. J. (1988) NMR spectroscopy of minerals and glasses. In *Spectroscopic Methods in Mineralogy and Geology*, Vol. 18 (ed. F. C. Hawthrone), pp. 341–403. Mineral. Soc. America.

Kohn S. C., Dupree R., and Smith M. E. (1989) Proton environments and hydrogen-bonding in hydrous silicate glasses from proton NMR. *Nature* **337,** 539–541.

Konijnendijk W. L. and Buster J. H. J. M. (1977) Raman-scattering measurements of silicate glasses containing sulfate. *J. Non-Cryst. Solids.* **23,** 401–418.

Köster C., Lindemann A., Kuchinke J., Mück-Lichtenfeld C., and Krebs B. (2002) Syntheses, crystal structures and vibrational properties of $Rb_4Si_4S_{10}$ and $Rb_4Si_4Se_{10}$. *Solid State Sci.* **4,** 641–650.

Luhr J. F. (1990) Experimental phase relations of water and sulfur-saturated arc magmas and the 1982 eruptions of El Chichon volcano. *J. Petrol.* **31,** 1071–1114.

Maekawa H., Maekawa T., Kawamura K., and Yokokawa T. (1991) The structural groups of alkali silicate glasses determined from ^{29}Si MAS NMR. *J. Non-Cryst. Solids* **127,** 53–64.

Matson D. W., Sharma S. K., and Philpotts J. A. (1983) The structure of high-silica alkali-silicate glasses: A Raman spectroscopic investigation. *J. Non-Cryst. Solids* **58,** 323–352.

McKeown D. A., Muller I. S., Gau H., Pegg I. L., and Kendziora C. A. (2001) Raman studies of sulfur in borosilicate waste glasses: Sulfate environments. *J. Non-Cryst. Solids.* **288,** 191–199.

McKeown D. A., Muller I. S., Gan H., Pegg I. L., and Stolte W. C. (2004) Determination of sulfur environments in borosilicate waste glasses using X-ray absorption near-edge spectroscopy. *J. Non-Cryst. Solids* **333,** 74–84.

McMillan P. F. (1994) Water solubility and speciation models. In *Volatiles in Magmas*, Vol. 30 (eds. M. R. Carroll and J. R. Holloway), pp. 131–156. Mineral. Soc. America.

McMillan P. F. and Wolf G. H. (1995) Vibrational spectroscopy of silicate liquids. In *Structure, Dynamics and Properties of Silicate Melts,* Vol. 32 (eds. J. F. Stebbins, P. F. McMillan and D. B. Dingwell), pp. 247–315. Mineral. Soc. America.

Métrich N. and Clocchiatti R. (1996) Sulfur abundance and its speciation in oxidized alkaline melts. *Geochim. Cosmochim. Acta* **60,** 4151–4160.

Métrich N., Bonnin-Mosbah M., Susini J., Menez B., and Galoisy L. (2002) Presence of sulfite (S-IV) in arc magmas: Implications for volcanic sulfur emission. *Geophy. Res. Lett.* **29,** doi:10.1029/2001GL014607.

Métrich N., Susini J., Galoisy L., Calas G., Bonnin-Mosbah M., and Menez B. (2003) X-ray microspectroscopy of sulfur in basaltic glass inclusions. Inference on the volcanic sulfur emissions. *J. Phys IV* **104,** 393–397.

Meyer B., Ospina M., and Peter L. B. (1980) Raman spectrometric determination of oxysulfur anions in aqueous systems. *Anal. Chim. Acta* **117,** 301–311.

Mysen B. O. and Popp R. K. (1980) Solubilities of sulfur in $CaMgSi_2O_6$ and $NaAlSi_3O_8$ melts at high pressure and temperature with controlled fO_2 and fS_2. *Am. J. Sci.* **280,** 78–92.

Mysen B. O., Virgo D., and Seifert F. A. (1982) The structure of silicate melts: Implications for chemical and physical properties of natural magma. *Rev. Geophys. Space Phys.* **20,** 353–381.

Mysen B. O. and Frantz J. D. (1992) Raman spectroscopy of silicate melts at magmatic temperatures: Na_2O-SiO_2, K_2O-SiO_2, Li_2O-SiO_2 binary compositions in the temperature range 25–1475°C. *Chem. Geol.* **96,** 321–332.

Mysen B. O. and Frantz J. D. (1994) Silicate melts at magmatic temperatures: In situ structure determination to 1651°C and effect of temperature and bulk composition on the mixing behavior of structural units. *Contrib. Mineral. Petrol.* **117,** 1–14.

Nagashima S. and Katsura T. (1973) The solubility of sulfur in Na_2O-SiO_2 melts under various oxygen partial pressures at 1100°C, 1250°C and 1300°C. *Bull. Chem. Soc. Japan.* **46,** 3099–3103.

Nakamoto K. (1986) *Infrared and Raman Spectra of Inorganic and Coordination Compounds.* Wiley.

O'Neill H. St. C and Mavrogenes J. A. (2002) The sulfide capacity and the sulfur content at sulfide saturation of silicate melts at 1400°C and 1 bar. *J. Petrol.* **43,** 1049–1087.

Paris E., Giuli G., Carroll M. R., and Davoli I. (2001) The valence and speciation of sulfur in glasses by X-ray absorption spectroscopy. *Can. Min.* **39,** 331–339.

Poulson S. R. and Ohmoto H. (1990) An evaluation of the solubility of sulfide sulfur in silicate melts from experimental data and natural samples. *Chem. Geol.* **85,** 57–75.

Shima H. and Naldrett A. J. (1975) Solubilities of sulfur in an ultramafic melt and the relevance of the system Fe-S-O. *Econ. Geol.* **70,** 960–967.

Shimazaki H. and Clark L. A. (1973) Liquidus relations in the FeS-FeO-SiO_2-Na_2O system and geological implications. *Econ. Geol.* **68,** 79–96.

Tatsumisago T., Hirai K., Hirata T., Takahashi M., and Minami T. (1996) Structure and properties of lithium ion conducting oxysulfide glasses prepared by rapid quenching. *Solid State Ionics* **86–88,** 487–490.

Tenhover M., Hazle M. A., and Grasselli R. K. (1983) Atomic structure of SiS_2 and $SiSe_2$ glasses. *Phys. Rev. Lett.* **51,** 404–406.

Wallace P. and Carmichael I. S. E. (1992) Sulfur in basaltic magmas. *Geochim. Cosmochim. Acta* **56,** 1863–1874.

Wallace P. and Carmichael I. S. E. (1994) S speciation in submarine basaltic glasses as determined by measurements of SKα X-ray wavelength shifts. *Am. Min.* **79,** 161–167.

Wells A. F. (1986) *Structural Inorganic Chemistry.* Oxford University Press.

Wendlandt R. F. (1982) Sulfide saturation of basalt and andesite melts at high pressures and temperatures. *Am. Min.* **67,** 877–885.

Xue X. and Kanzaki M. (2004a) Stability and NMR characteristics of possible sulfur species in silicate melts and glasses: An ab initio

calculation. In *Proceedings for the XX International Congress on Glass*.

Xue X. and and Kanzaki M. (2004b) Dissolution mechanisms of water in depolymerized silicate melts: Constraints from ^{1}H and ^{29}Si NMR spectroscopy and ab initio calculations, *Geochim. Cosmochim. Acta*, **68**(*24*), 5027–5057.

Xue X., Stebbins J. F., Kanzaki M., Poe B., and McMillan P. (1991) Pressure-induced silicon coordination and tetrahedral structural changes in alkali oxide-silica melts up to 12 GPa: NMR, Raman and infrared spectroscopy. *Am. Min.* **76,** 8–26.

Xue X. and Stebbins J. F. (1993) ^{23}Na NMR chemical shifts and local Na coordination environments in silicate crystals, melts and glasses. *Phys. Chem. Min.* **20,** 297–307.

Yasuda A., Nakada S., and Fujii T. (2001) Sulfur abundance and redox state of melt inclusions from Miyake-jima 2000 eruption products. *Bull. Volcanol. Soc. Jpn.* **46,** 165–173.